

AD-A134 597

12

Report No. HA 111-83

FINAL REPORT ON  
HYDROSHOCK<sup>(R)</sup> WATER GUN RESEARCH

April 5, 1983

DTIC  
ELECTE  
NOV 10 1983  
S B

DTIC FILE COPY

DISTRIBUTION STATEMENT A

Approved for public release  
Distribution Unlimited

HYDROACOUSTICS INC.

83 11 09 050

Report No. HA 111-83

FINAL REPORT ON  
HYDROSHOCK<sup>(R)</sup> WATER GUN RESEARCH

April 5, 1983

Submitted to:

Office of Naval Research  
800 North Quincy Street  
Arlington, Virginia 22217

Attention: Dr. Peter Rogers, Code 425

Contract N00014-82-C-0647

**HYDROACOUSTICS INC.**

999 LEHIGH STATION RD. P.O. BOX 23447 ROCHESTER, N.Y. 14692

TABLE OF CONTENTS

<u>Section</u>	<u>Page</u>
1.0 <u>INTRODUCTION</u>	1-1
2.0 <u>DESCRIPTION OF THE SOURCE</u>	2-1
3.0 <u>HIGH-SPEED MOTION PICTURES</u>	3-1
3.1 Setup for Movies	3-1
3.2 Cavitation Histories	3-3
4.0 <u>ENERGY UTILIZATION</u>	4-1
5.0 <u>SENECA LAKE MEASUREMENTS</u>	5-1
6.0 <u>DISCUSSION OF RESULTS</u>	6-1
7.0 <u>RECOMMENDATIONS</u>	7-1
8.0 <u>REFERENCES</u>	8-1
9.0 APPENDIX	9-1

LIST OF FIGURES

<u>Figure</u>	<u>Page</u>
2.1 Hydroshock Water Gun	2-2
2.2 Hydroshock Water Gun Operation	2-4
2.2A Latched	2-4
2.2B Fired	2-4
2.2C Cut-Off	2-4

LIST OF FIGURES(Continued)

<u>Figure</u>		<u>Page</u>
3.1	Setup for High-Speed Movie of Underwater Cavity History	3-2
3.2	Selected Movie Frames Showing Cavitation Bubble History for Hydroshock Gun with Round Ports	3-4 3-4A
3.3	Selected Movie Frames Showing Cavitation Bubble History for Hydroshock Gun with Rectangular Ports	3-7 3-7A
3.4	Pressure Waveform Oscillograph for Water Gun with Round Ports	3-9
3.5	Pressure Waveform Oscillograph for Water Gun with Rectangular Ports	3-10
3.6	Radius-Time Curve for Round Ports	3-11
3.7	Radius-Time Curve for Rectangular Ports	3-13
3.8	Frontal Excursion Vs. Time for Round Ports	3-14 -
3.9	Frontal Excursion Vs. Time for Rectangular Ports	3-15
3.10	Port Opening Vs. Time	3-17
4.1	Computer Simulation of Jet Energy Accumulation	4-4
5.1	Pressure Waveform from the Time of Solenoid Energization	5-2
5.2	Pressure Waveform with Gun 90 Feet Deep	5-4
5.3	Pressure Waveform with Gun 150 Feet Deep	5-5
5.4	Pressure Waveform with Gun 210 Feet Deep	5-6
5.5	Pressure Waveform with Gun 280 Feet Deep	5-7
5.6	Pressure Waveform with Gun 305 Feet Deep	5-8
5.7	Peak Source Level Vs. Depth	5-10
5.8	Peak Source Level Vs. Peak Air-Spring Pressure	5-11

LIST OF TABLES

<u>Table</u>	<u>Page</u>
2.1 Characteristics of Hydroshock <sup>(R)</sup> Model HS-56 Water Gun	2-3
4.1 Energy Utilization by Hydroshock <sup>(R)</sup> Model HS-56 Water Gun	4-2

Accession For	
NTIS GRA&I	<input checked="" type="checkbox"/>
DTIC TAB	<input type="checkbox"/>
Unannounced	<input type="checkbox"/>
Justification	
By _____	
Distribution/	
Availability Codes	
Dist	Avail and/or Special
A-1	



## 1.0 INTRODUCTION

This report presents the results of an investigation into some of the factors which control the performance of the water gun as an acoustic source. The work is based upon observations of the Hydroshock<sup>(R)</sup> Model HS-56 water gun which Hydroacoustics has developed over several years. This source generates a clean, broadband signal which is attractive for relatively high resolution acoustic profiling and in target strength measurement.

The source and its operation are described in Section 2.0. The use of high-speed movies to study the phenomenon of the growth and collapse of the cavitation bubble generated by the gun is presented in Section 3.0.

Section 4.0 covers a stagewise analysis of the energy utilization as it passes through the source. This work depends in part upon measurements made on the high-speed movies. It also employs a computer simulation of the operation of the water gun which is described.

Measurements of the performance of the gun as a function of operating depth and of internal air-spring pressure are described in Section 5.0. These acoustic measurements were made at gun depths to 305 feet in Seneca Lake, NY. Section 6.0 is a discussion of the results. Recommendations are presented in Section 7.0.

An analysis of the operation of the water gun as an acoustic generator prepared by Dr. H. G. Flynn is presented in the Appendix in Section 9.0.

(R) Registered Trademark

## 2.0 DESCRIPTION OF THE SOURCE

The Hydroshock<sup>(R)</sup> water gun is a repetitive underwater impulse generator powered by high-pressure water. It converts the potential energy of compressed air into the kinetic energy of high-velocity water jets, then into the potential energy of underwater cavitation voids and ultimately into the acoustic energy generated by violent implosion of the cavitation voids. (References 1 and 2).

The source produces a clean impulsive signature with a far-field peak source level greater than 5 bar-meters (234 dB re 1 $\mu$  Pa @ 1m) in a 0 to 5000 Hz band. Most of the energy is below 2000 Hz.

The source is powered by a 15-hp triplex pump and is triggered by a dc voltage from the source controller to the solenoid valve on the gun.

The gun is shown in Figure 2.1. The solenoid valve is seen at the top of the gun with its electrical connector. The uppermost item, except for the towing bail, is the fitting to which the high-pressure water hose attaches. One of the four round ports for the high-velocity water jets is visible. The rectangular port just below the top flange is a passive vent. The high pressure air spring occupies the lower portion of the cylindrical body. The device is held together by the tie rods.

The characteristics of the gun are summarized in Table 2.1. In this work, only the eight-inch piston stroke was used, giving a piston displacement of 56 cubic inches.

Operation of the source is illustrated in Figure 2.2. With pressure in the sleeve valve chamber, the sleeve valve is forced shut. Then high pressure seawater introduced into the water chamber cocks the piston, compressing the air in the air chamber (Figure 2.2A). To fire the gun, the solenoid valve is switched, dropping the pressure in the sleeve valve chamber to ambient, allowing the sleeve valve to open. The high pressure water operates on the end of the sleeve valve, accelerating the valve to its fully opened position (Figure 2.2B).



Figure 2.1 HYDROSHOCK Water Gun

TABLE 2.1  
CHARACTERISTICS OF HYDROSHOCK<sup>(R)</sup> MODEL HS-56 WATER GUN

Model	HS-56
Hydraulic Fluid	Water
Displacement	35 or 56 cu. in.
Piston Diameter	3 inches
Piston Stroke	5 or 8 inches
Exhaust Port Area, Round Ports	1.77 sq. in.
Exhaust Port Area, Rectangular	4.79 sq. in.
Peak Air Pressure, Cocked	2400 psi
Hydraulic Pressure	2800 psi
Length	51 inches
Weight In Air	125 lb

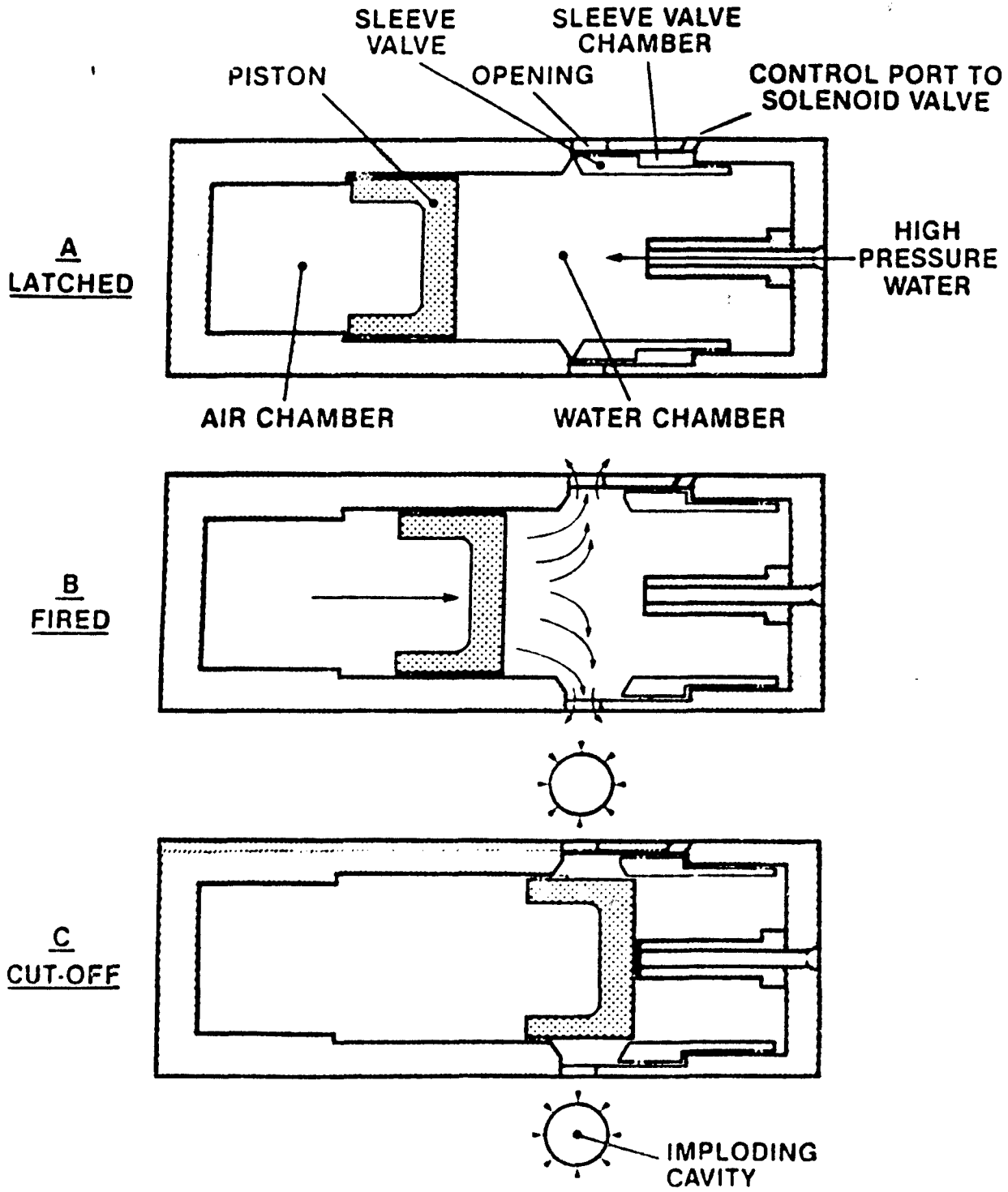


Figure 2.2 HYDROSHOCK Water Gun Operation

The high pressure air in the air chamber accelerates the piston which pushes water out of the ports at high velocity until the piston crosses over the ports, abruptly terminating the outward flow through the four ports. (Figure 2.2C). Cavitation voids, which are formed by each of the four jets, grow and subsequently collapse violently creating the acoustic pulse. The piston is decelerated in a controlled manner in the forward water-filled cavity which forms a dashpot. By powering the device with water instead of compressed air, operating efficiency is estimated to be increased by an order of magnitude.

### 3.0 HIGH-SPEED MOTION PICTURES

The underwater movies were directed principally toward obtaining a pictorial history of the growth and collapse of a single one of the four underwater cavities formed when the gun is fired.

#### 3.1 SETUP FOR MOVIES

The general arrangement of the water gun and photographic equipment for a typical movie record is shown in Figure 3.1. The depth of the gun in the water is defined as the depth of the port beneath the surface. The movie camera was focussed on the site of one cavity (the cavity nearest the reader in Figure 3.1). The axis of the subject cavity was perpendicular to the photographic axis. The viewing box with an acrylic window was used to avoid surface ripples.

Backlighting was provided by an underwater flash lamp box which was perpendicular to and centered on the photographic axis behind the subject cavity. A maximum of ten Sylvania type FF33 magnesium-filament flash lamps could be fired simultaneously in this light source. One of these lamps produces an average usable lumen level of 55,000 lumens for a duration of 2.5 seconds.

As many as twelve 600-watt aircraft landing lamps were used above the surface to provide frontal illumination on the underwater cavity.

The photography was performed by Mr. A Earl Quinn, high-speed photography specialist, formerly of Eastman Kodak Company. He used a Redleg Hy-Cam, 16 mm movie camera capable of 11,000 frames per second. Speeds from 2000 to 6000 frames per second were used with apertures from f/4 to f/8. The high-speed color film was Ektochrome, ASA 400.

During exposure, the edge of the movie film also is exposed to a timing light within the camera which flashes 120 times per second to permit calibration of the frame rate throughout the roll of film.

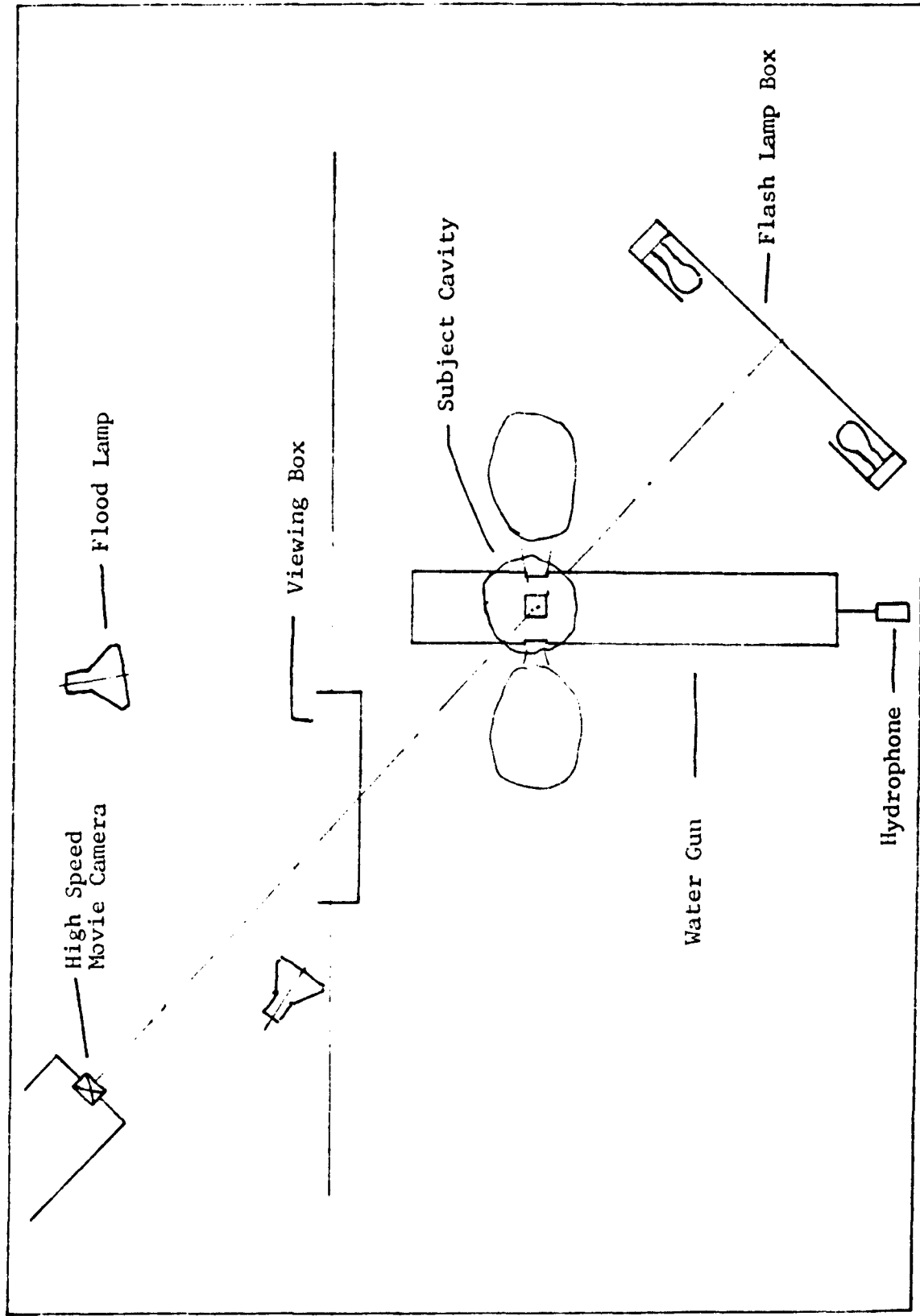


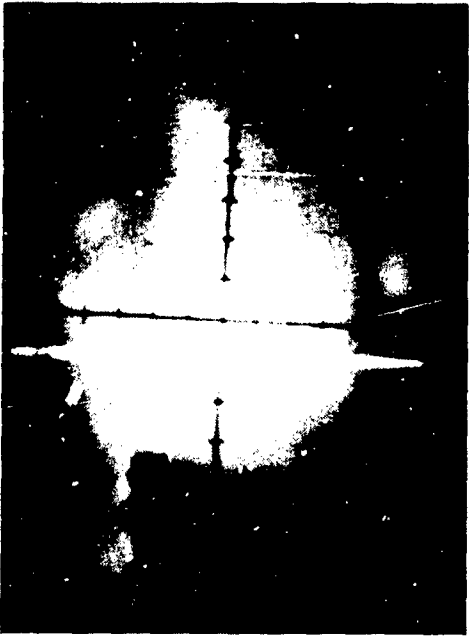
Figure 3.1 Setup for High-Speed Movie of Underwater Cavity History

In addition to the conventional lens which views the cavity of the water gun, a second lens specially installed in the rear of the high-speed camera views the screen of an oscilloscope located behind the camera. This screen displays the acoustic pressure in the water as recorded by a hydrophone beneath the water gun. The uniaxial oscilloscope display is a single point on the screen which moves horizontally in proportion to the magnitude of the acoustic pressure, the time sweep of the oscilloscope having been disconnected. This view is projected continuously through the back of the movie film onto the emulsion during exposure. To the movie viewer, the acoustic pressure appears as a vertical white trace superimposed on all frames in the roll. See Figure 3.2.

The flood lamps and the oscilloscope were turned on prior to each shot. However, the high-speed camera, the flash lamps, and the water gun itself, required synchronization. Depending on the frame rate used, the camera requires a significant part of a second to reach full speed. The lumen level of the flash lamps peaks about 3/4-second after their ignition. The formation and collapse of the cavities associated with the water occur between 15 and 60 milliseconds following energization of the solenoid valve on the gun. After initial trials, the camera and flash lamps were synchronized manually by the photographer. The water gun was automatically triggered by the camera after a preset portion of the roll of film was exposed.

### 3.2 CAVITATION HISTORIES

Shown in Figure 3.2 is a series of selected movie frames which record the history of the cavitation bubble for the Hydroshock<sup>(R)</sup> water gun fitted with four round ports, each 0.75-inches in diameter. Throughout this study, the piston stroke was 8 inches resulting in a 56-cubic-inch displacement. The air spring was precharged to 1800 psig and the gun ports were 21 inches below the surface. The side of the gun forms the left side of the frame. Lighting was solely by surface flood lamps. For this roll, the water pumped into the gun was treated with a red food coloring.



Frame 6 3.3 ms (emission start)



Frame 41 22.8 ms



Frame 15 8.9 ms (emission finish)



Frame 42 23.3 ms





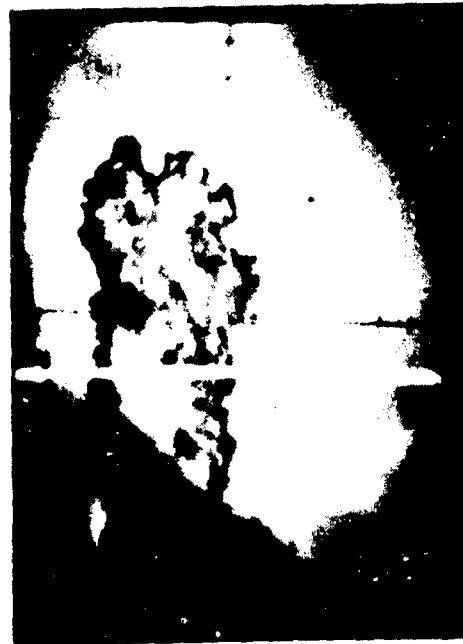
Frame 50 27.8 ms



Frame 55 30.6 ms



Frame 25 15.6 ms



Frame 35 18.8 ms (max. cavity)

Figure 3.2 Selected Movie Frames Showing Cavitation Bubble History for Hydroshock® Water Gun with Round Ports 1 of 2

1 2



Frame 56 31.1 ms (min. cavity)



Frame 70 38.8 ms



Frame 57 31.7 ms (max. pressure)



Frame 79 43.9 ms (2nd min. cavity)



NOTES: Roll No. 12, 1800 frames per second. Vertical white line is continuous trace of acoustic pressure. Positive pressure causes deflection to the right. Gun pre-

Roll No. 12, 1800 frames per second. Vertical white line is continuous trace of acoustic pressure. Positive pressure causes deflection to the right. Gun pre-charge air pressure is 1800 psig. Each of four ports is 0.75 inches diameter. Water depth of port is 21 inches.

NOTES:



Frame 59 32.8 ms



Frame 65 36.1 ms

Figure 3.2 Selected Movie Frames Showing Cavitation Bubble History for Hydroshock® Water Gun with Round Ports 2 of 2

3-4A

1 2

At 1800 frames per second, the frames are 0.56 milliseconds apart. Emission of the jet from the port is first observed in Frame 6. In Frame 15, 6.6 msec later, we see the cessation of the emission. The dark area below the port end of the cavity in Frame 15, appears abruptly in each film sequence about 6 or 8 milliseconds after emission starts. It appears to result from a brief jet of extra-high-velocity water diverted downward relative to the principal jet axis as the sleeve valve closes the port. If so it is an accurate indication of jet cutoff. The observed volume of the cavity then at each port is 57 cubic inches. By contrast, the water ejected from each port is 14 cubic inches. Thus, by the time of emission cutoff, the volume of the resultant cavity is already four times the volume of the water jet which spawned it.

The cavity volume grows to a maximum in Frame 35 and begins to contract. In Frame 55, the vertical white trace has started to move to the right indicating positive acoustic pressure. In Frame 56, 27.8 msec after initial emission, this cavity has collapsed to the minimum observed volume. In Frame 57, the maximum positive acoustic pressure excursion from the hydrophone trace is observed. This occurs 0.6 msec after the minimum cavity is photographed because the hydrophone is 38 inches from the center of the imploded cavity.

Many small dark spots are seen in Frame 57. This is attributed to small nuclei at the surface viewing window, which suddenly expand under the influence of the rarefaction wave created by the inversion of the positive pressure pulse when it reaches the surface.

A maximum negative pressure swing is observed in Frame 59, about 1.6 frames or 0.9 msec after the positive peak. This interval is approximately the round trip time of the positive pressure pulse which is reflected and inverted by the surface 21 inches above the port. A second minimum cavity is seen in Frame 79.

The overall shape of this cavitation bubble throughout its existence is relatively elongated and somewhat irregular. We note the inverted vee front which persisted from Frame 25 onward. These views are downward 45 degrees from the vertical. This inverted-vee front was even more evident from a top view of the cavity.

Another cavitation bubble history is shown in Figure 3.3 for the water gun fitted with four rectangular ports which provide 2.3 times the port area of the round ports. The frame rate, gun depth, and air precharge pressure, match those of the previous figure. The illumination, in this case, however, includes flash lamps behind the cavity as well as flood lamps for front lighting.

Emission starts in Frame 3 and stops in Frame 14, lasting 6.3 msec. At the time of emission cutoff, the observed volume of the cavitation void is 123 cubic inches or about nine times the volume of water emitted from this port. This compares with only four times the water in the cavity at cutoff in the previous case of the smaller ports in Figure 3.2. This possible inconsistency may imply that cutoff occurred somewhat earlier than judged from Figure 3.3.

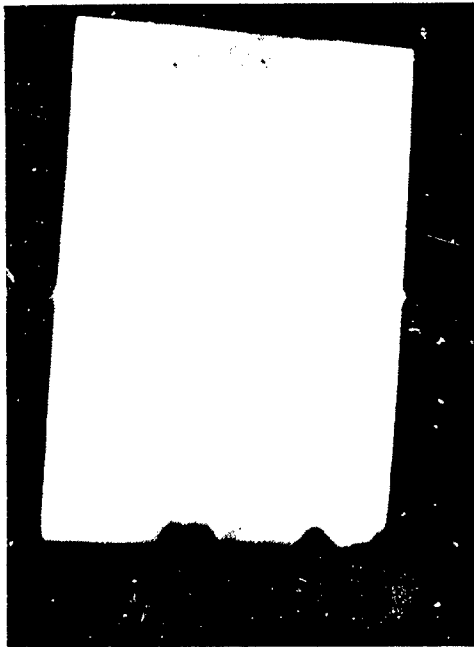
The cavity reaches a maximum volume in Frame 30. The minimum cavity appears to have been precisely recorded in Frame 54. The positive acoustic pressure pulse, which begins in Frame 54, is approaching a high peak as it leaves the top of Frame 55. The eruption of surface nuclei is also seen in Frame 55. The cavity is seen to re-expand to a second maximum volume in Frame 68 followed by a second minimum volume in Frame 76. A third maximum cavity is seen in Frame 78. The relatively minimal contribution to the acoustic waveform of these secondary cavity oscillations will be shown later.



Frame 20 11.5 ms



Frame 30 17.2 ms (max. cavity)



Frame 3 1.7 ms



Frame 6 3.4 ms



Frame 40 23.0 ms



Frame 50 28.7 ms



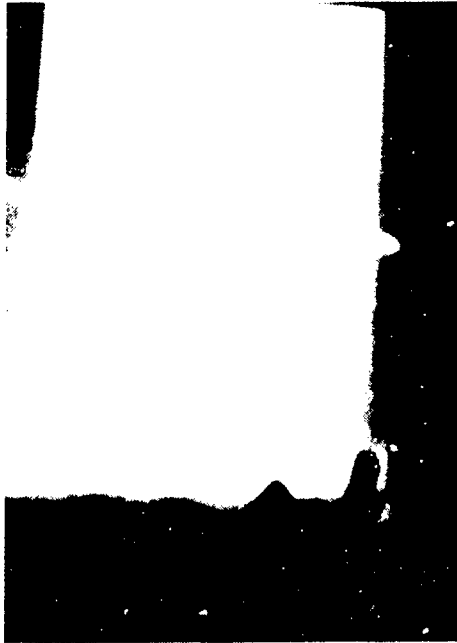
Frame 9 5.2 ms



Frame 14 8.0 ms (end of emission)

Figure 3.3 Selected Movie Frames Showing Cavitation Bubble History for Hydroshock® Water Gun with Rectangular Ports 1 of 2

2



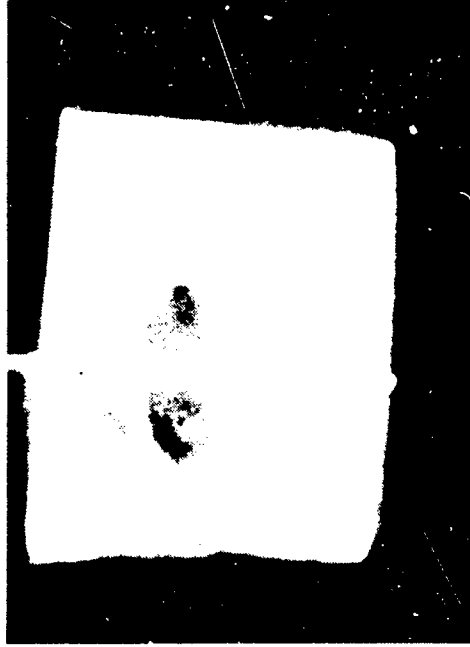
Frame 54 31.0 ms (min. cavity)



Frame 76 43.7 ms (2nd min. cavity)



Frame 55 31.6 ms (max. pressure)



Frame 78 44.8 ms (3rd max. cavity)



NOTES: Roll No. 18, 1740 frames per second. Vertical white line is continuous trace of acoustic pressure. Positive pressure causes deflection to the right. Gun pressure is 1000 psi. Each of four...

**NOTES:** Roll No. 18, 1740 frames per second. Vertical white line is continuous trace of acoustic pressure. Positive pressure causes deflection to the right. Gun pre-charge air pressure is 1800 psig. Each of four ports is 1 x 1.25 inches. Water depth to the port is 21 inches.



Frame 59 33.9 ms



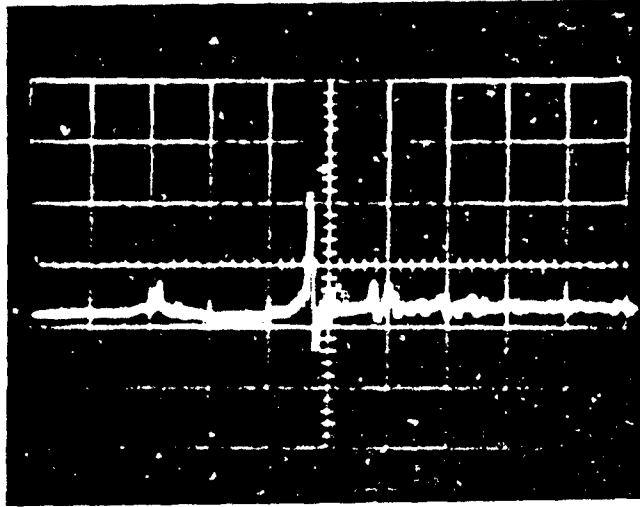
Frame 68 39.1 ms (2nd max. cavity)

Figure 3.3 Selected Movie Frames Showing Cavitation Bubble History for Hydroshock® Water Gun with Rectangular Ports 2 of 2

The inverted vee front on the cavity is seen in Frames 14, 20, and 30. The camera angle is about 45 degrees down for this roll. The vee front was more evident from top views of the cavity. However, this phenomena was more prominent in the cavity for the gun with round ports.

The cavity shape is more regular and more nearly spherical for these larger rectangular ports (total area 4.79 square inches) than for the smaller round ports (total area 1.77 square inches).

The acoustic pressure waveform which was superimposed on the movie film, was simultaneously recorded on the oscillograph for each shot. Figure 3.4 is the oscilloscope record of the event in Figure 3.2 for the gun with round ports. The measurement hydrophone was close beneath the source, on the axis of the source, placing it about 35 inches equidistant from each of the four cavities at their collapse. Energization of the solenoid valve which fires the gun initiates the oscilloscope sweep. The first pressure deflection at 17 msec is associated with initiation of the jet emission when the sleeve valve starts to open. The subsequent growth and collapse of the cavity is terminated at the implosion indicated by the major positive pressure peak at 47 msec. The negative swing in the next msec is the surface reflection. Two small positive pulses beginning 11 msec after the main pulse are believed to be associated with secondary cavity collapses. This time record of the event may be compared directly with the record in Figure 3.2



Legend: Vertical Scale: 2 bar meters/div  
Horizontal Scale: 10 msec/div  
Band: 0 - 2000 Hz  
Separation: 38 inches  
4 Round Ports  
1800 psig air precharge pressure  
Reference: Roll No. 12

Figure 3.4 Pressure Waveform Oscillograph For  
Water Gun With Round Ports

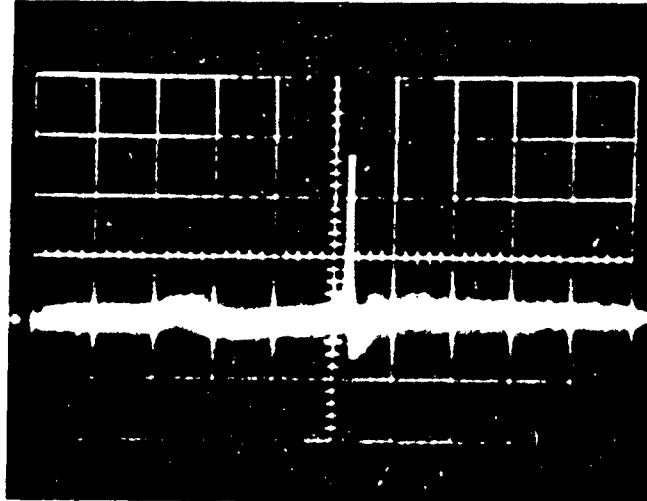
The pressure waveform for the gun with rectangular ports is shown in Figure 3.5. Initial deflection indicating initial opening of the sleeve valve is seen at 20 msec into the sweep. Cavity collapse occurs at 52.5 msec. Since this 32.5 msec duration from jet initiation to implosion is longer than the 30 msec observed in the case of the round ports, it implies that there is more energy in the cavity formed with the rectangular ports.

A cavitation bubble is well defined by the history of its volume. Figure 3.6 is a plot of the equivalent radius of the cavity as a function of time for the gun with round ports. This is the radius of a sphere whose volume is that of the cavity observed in the high-speed movie. For these measurements, the cavity is assumed to be a spheroid whose diameter (D) is its height on the movie screen and whose length (L) is its width in the screen. With appropriate scale corrections, the equivalent radius (R) is computed as follows:

$$R = 1/2 (L \times D^2)^{1/3}$$

The radius time plot of Figure 3.6 is taken from the movie film shown in Figure 3.3. The plot indicates a maximum equivalent radius of about four inches and a cavity decay time from maximum radius to collapse of about 12 msec. As measured from the movie, the secondary cavity is relatively large. However, its acoustic significance is much less according to the pressure waveform in Figure 3.4.

Figure 3.7 is the radius-time curve for the gun under similar conditions with rectangular ports. It is derived from the movie of Figure 3.3. The maximum equivalent radius is about 4.15 inches with a decay time of about 12 msec. The minimum radius at collapse is quite small. The size of the secondary cavity is somewhat less than was the case for round ports.



Legend: Vertical Scale: 1.85 bar meters/div  
Horizontal Scale: 10 msec/div  
Band: 0 - 2000 Hz  
Separation: 35 inches  
4 Rectangular Ports  
1800 psig air precharge pressure  
Reference: Roll No. 18

Figure 3.5 Pressure Waveform Oscillograph For  
Water Gun With Rectangular Ports

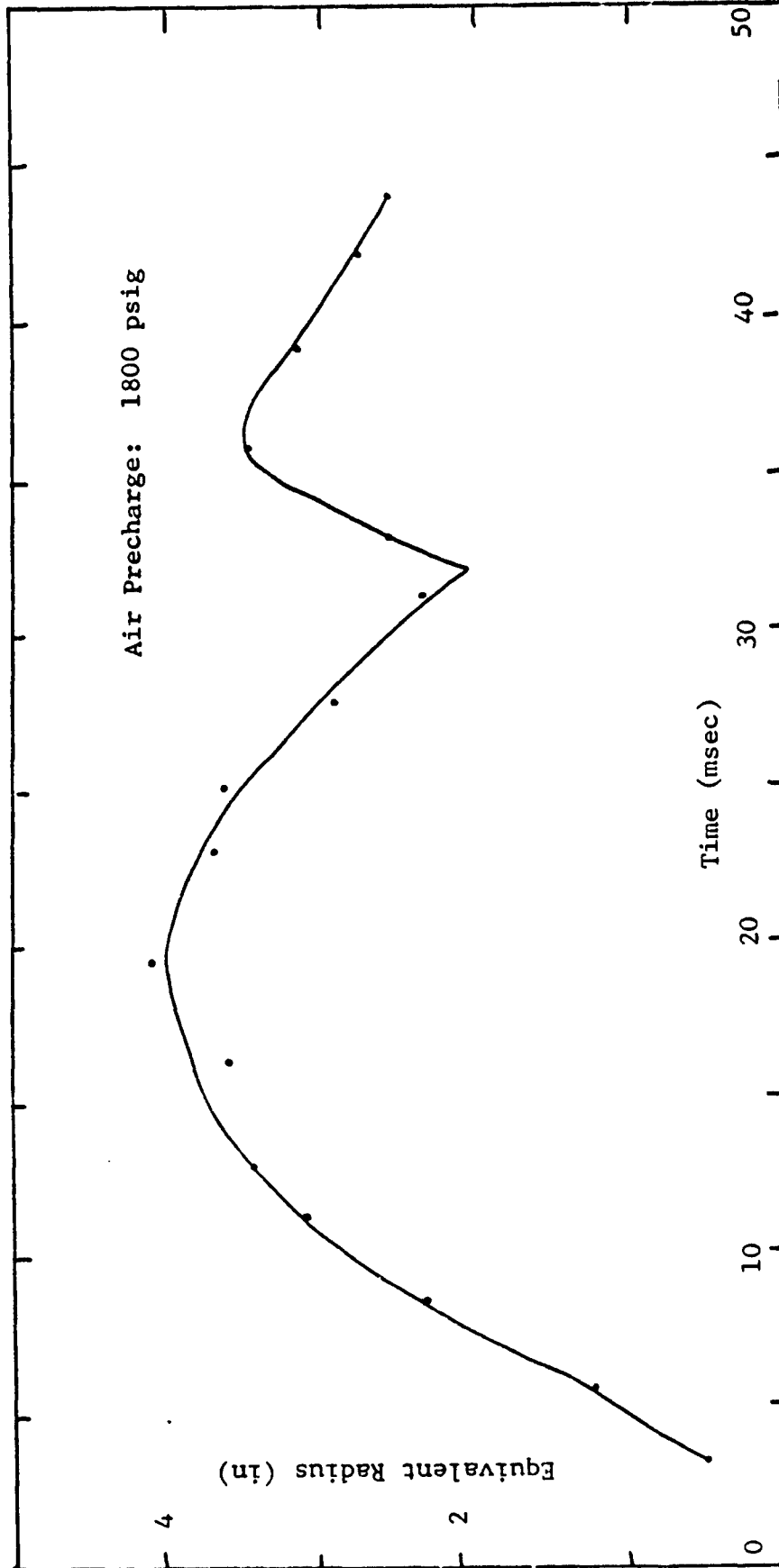


Figure 3.6 Radius-Time Curve for Round Ports

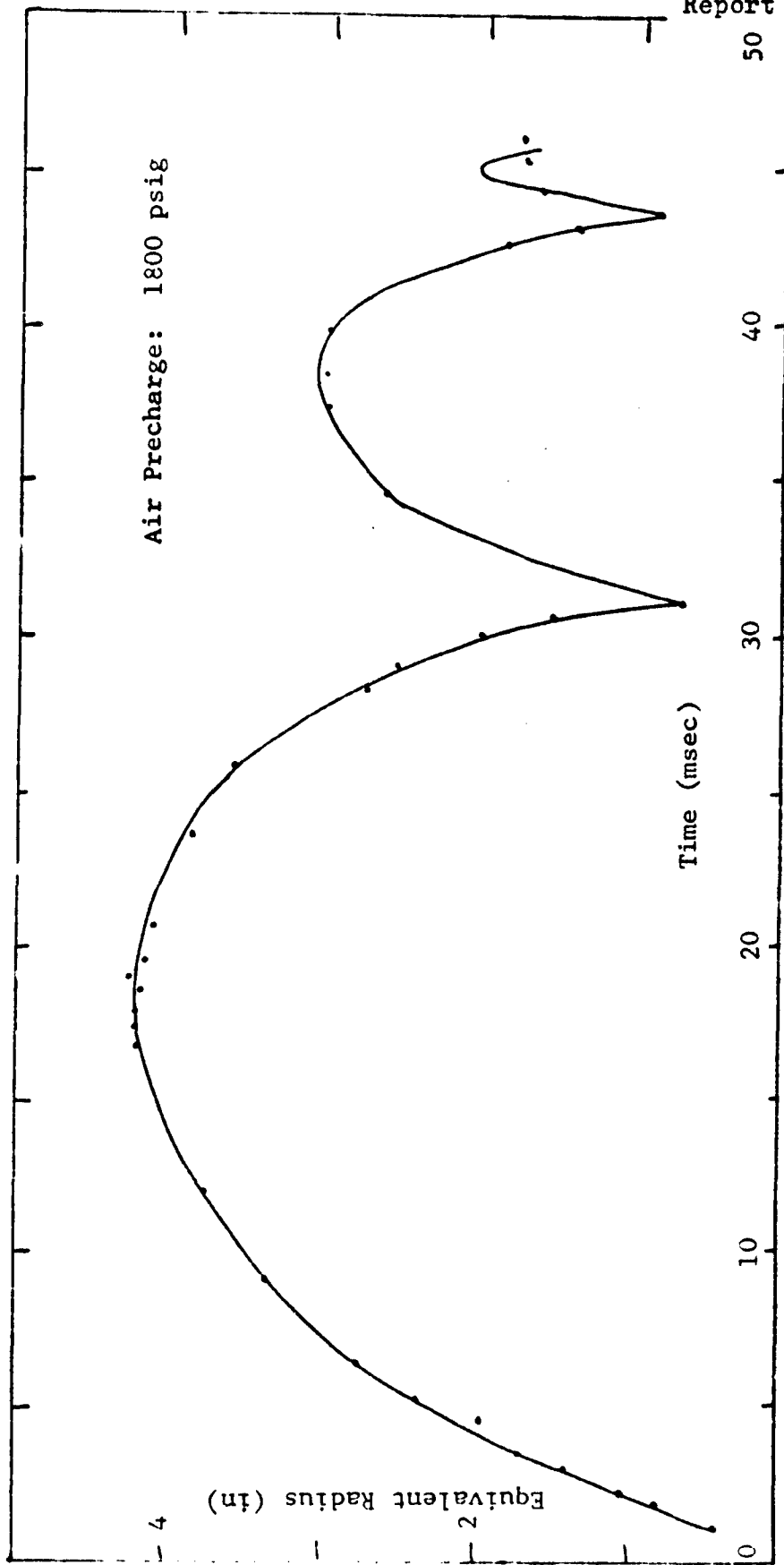


Figure 3.7 Radius-Time Curve for Rectangular Ports

The excursion of the cavity front as a function of time is shown in Figure 3.8 for the gun with round ports. The measurements are taken from the film roll of Figure 3.2. The cavity front moves about 18 inches out from the gun in a gradually decelerating manner.

Figure 3.9 presents the frontal excursion of the cavity vs. time for the gun with rectangular ports. When the front reaches 15 inches from the gun, the leading whisp dies out and cavity front translation ceases. This occurs about 17 msec after the start of emission, when the cavity is reaching its maximum volume. A velocity maximum is seen between 6 and 7 msec, about the time the piston travel is closing off the jet port.

The high-speed movie camera proved useful in observing the performance of operating components of the gun itself. The speed at which the jet port opens is of particular interest. The sleeve valve is accelerated upward to uncover the ports and allow emission of the jet. Cavitation of the jet prevents observation of the port opening action directly. However, the upper end of the sleeve valve is visible through passive relief ports near the top end of the gun. The result of photographing and viewing the sleeve valve through this upper port is tabulated in Figure 3.10. Observations of the position of the sleeve valve vs. time indicate that the main jet port is uncovered in a little over 3 msec. This confirmed the acceleration predicted for the sleeve valve and subsequently utilized in the mathematical simulation of the gun's action.

Other film footage verified the timely operation of the solenoid valve and the exhaust from the sleeve drive cavity.

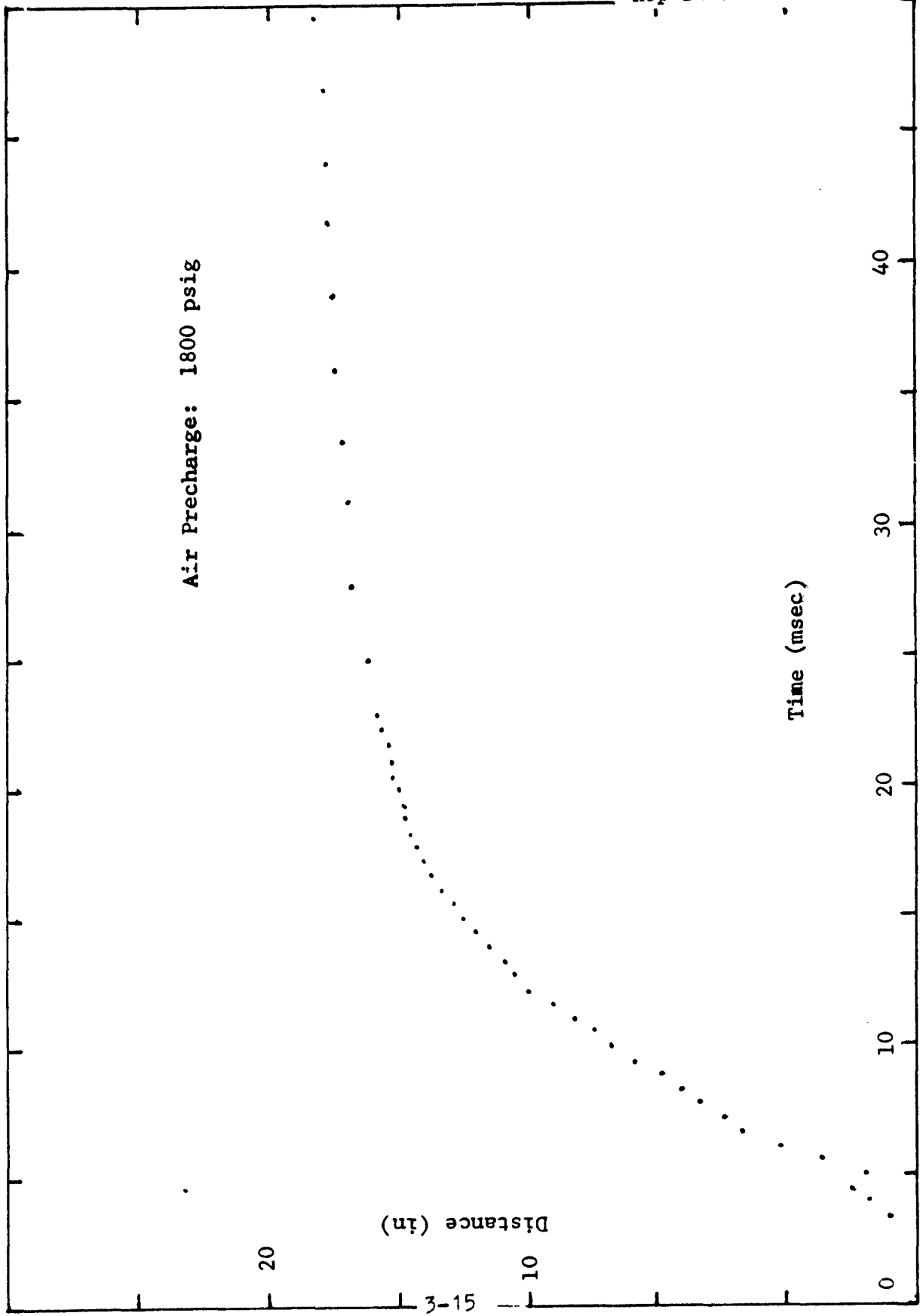


Figure 3.8 Frontal Excursion vs. Time for Round Ports

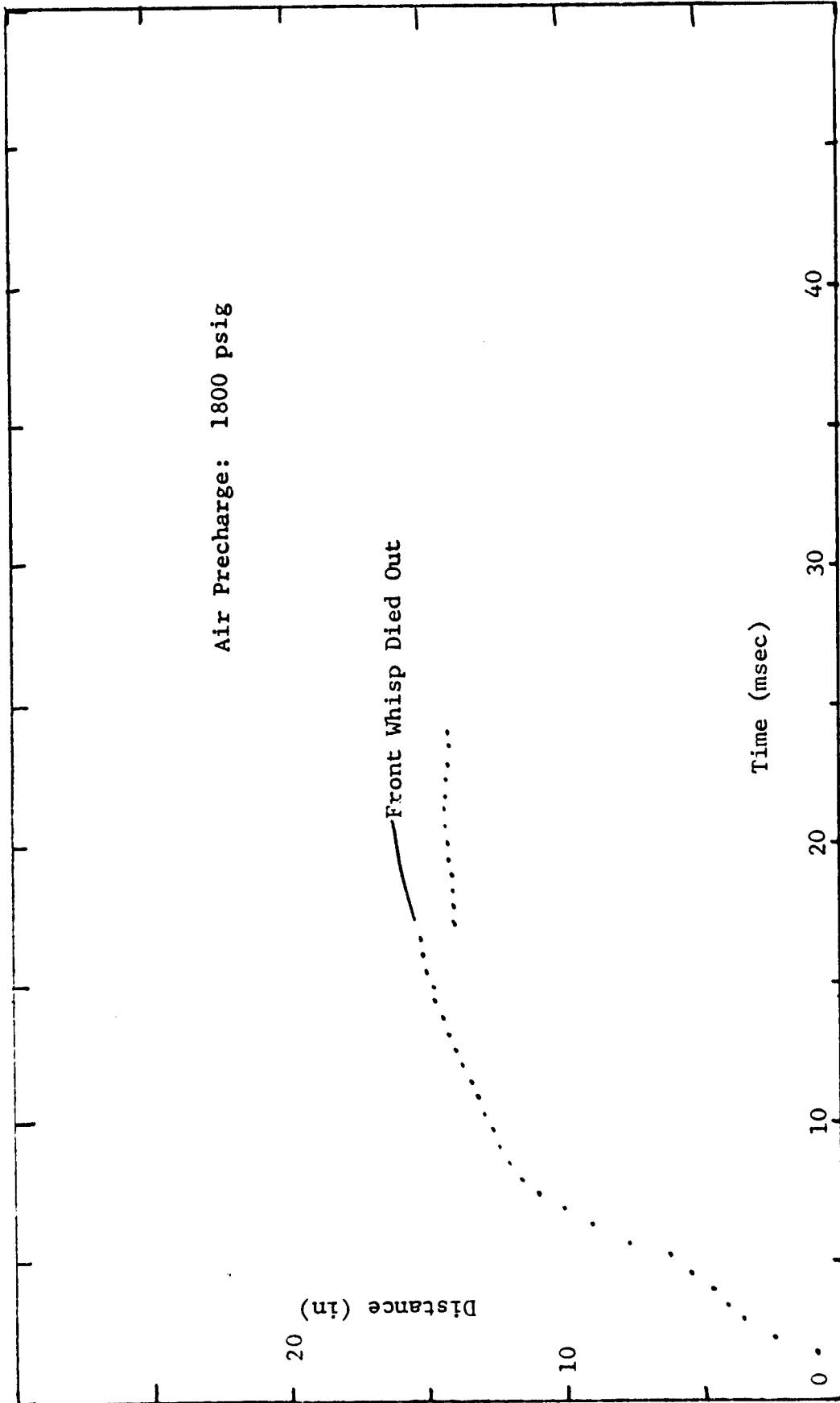


Figure 3.9 Frontal Excursion vs. Time for Rectangular Ports

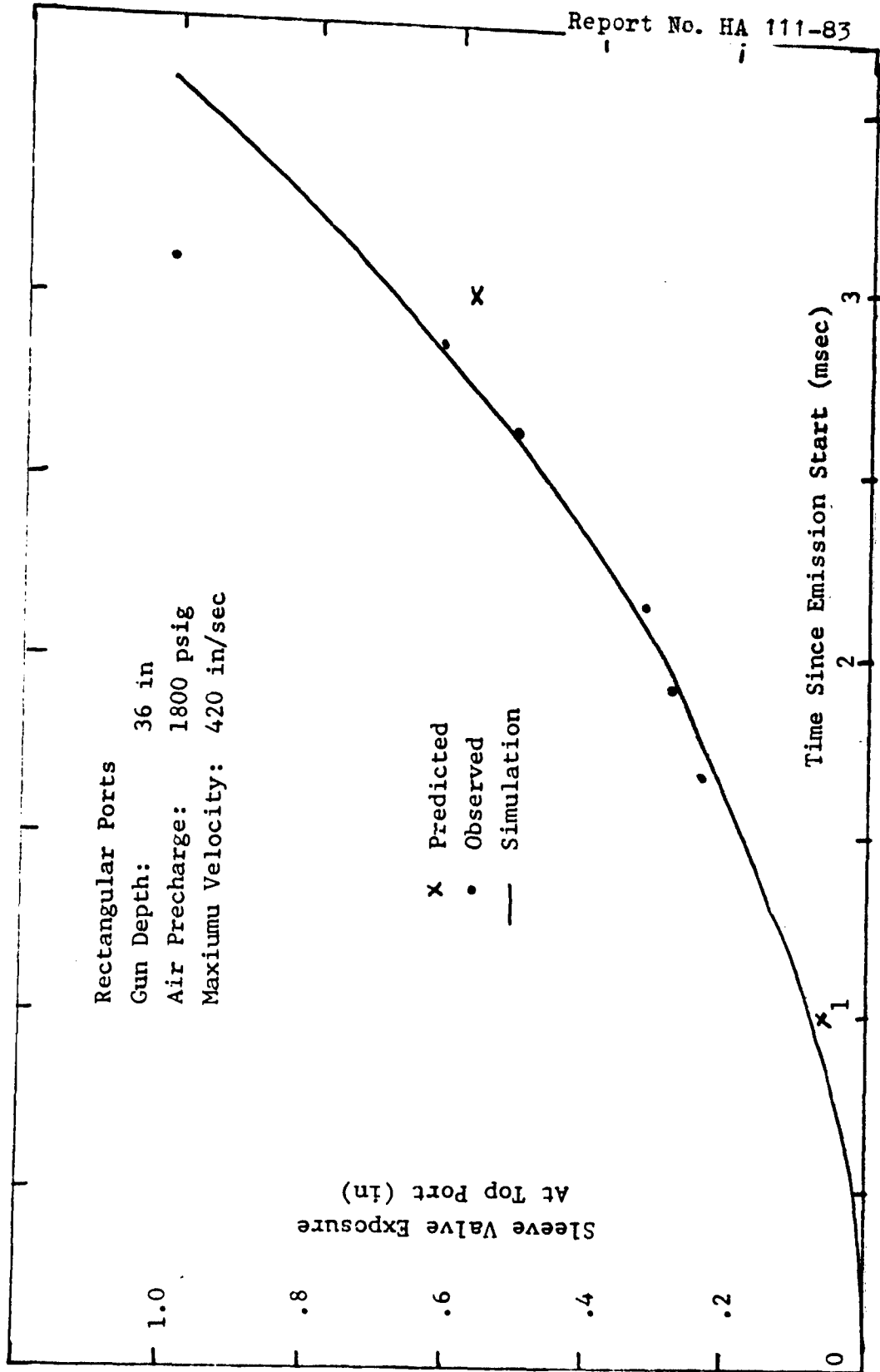


Figure 3.10 Port Opening vs. Time

#### 4.0 ENERGY UTILIZATION

It is enlightening to determine the utilization of the input energy as it passes through the gun. Table 4.1 contains estimates of the amount of energy identifiable at various stages in the gun. The base line operating conditions which were obtained for the shot recorded on Roll 18 (Figure 3.3) are utilized.

The input energy per shot is identifiable at the pump output where the pressure, flow rate, and minimum cocking time are well-known. Electric motor input and output were derived from pump and motor efficiencies.

The energy to compress the air spring and the energy released during its expansion were estimated by the simplifying assumptions of slow isothermal compression during cocking and rapid adiabatic expansion when the gun is fired.

The kinetic energy delivered to the jets was derived from a computer simulation of the operation of the water gun. This simulation accounted for the expansion of the air in the air spring, the mass of the piston, the mass of the water within the gun, the friction of the piston seals, and the orifice drop of the water jets exiting through the ports. The motion of the sleeve valve in uncovering the ports, as shown in Figure 3.10, was simulated. The port closing action by the moving piston near the end of the piston stroke, as depicted in Figure 2.2C, was also modeled. Impedance to flow of the water jet outside the port was ignored in the simulation.

TABLE 4.1  
 ENERGY UTILIZATION BY  
 HYDROSHOCK<sup>(R)</sup> MODEL HS 56 WATER GUN

CONDITIONS: Rectangular ports, 1800 psig air  
 precharge, 8-inch stroke, 21-inch  
 depth. Reference - Roll 18

<u>Stage</u>	<u>Joules per Shot</u>
Pump Delivery	
6.5 gpm @ 2300 psi, 3 sec/shot	
Eff = 0.8	19,500
Air Spring Compression	
Isothermal, 1816 - 2415 psia	13,500
Air Spring Expansion	
Adiabatic, 2415 - 1009 psia	10,200
Kinetic Energy in Jets (4)	
From simulation	7,820
Potential Energy of Max. Cavity(4)	
4.18 in radius, 21 in. deep	2,140
Acoustic Energy, Positive Pulse	
Triangular, 5.2 bar meter,	
1.3 msec duration	950
Potential Energy of Second Max.	
Cavity, 3 inch radius (4)	790

Shown in Figure 4.1 is the computer-derived curve of cumulative kinetic energy in the jets as a function of time. We see that the most rapid transmission of energy from the gun via the jets occurs during the period when the piston is beginning to close the jet ports. The computed instantaneous peak power is 7.2 megawatts. At that time the pressure inside the gun rises rapidly, the jet velocity accelerates, and kinetic energy in the moving piston is extracted as it is decelerated. From seven to well beyond 20 msec, the cumulative jet energy increases slowly at an even decreasing rate. While this effect itself is insignificant, it tends to validate the simulation. After rapidly closing the ports, the piston enters an increasingly closer-fitting dash pot. This decelerates the piston to avoid sharp impact at the top end of the stroke.

After seven msec, the ports are closed and most of the gun's energy has been expelled. This compares with a 6.3-msec emission period observed in the movie for this case (Figure 3.3). We have chosen the cumulative jet energy at this time for use in Table 4.1.

The measured energy in the positive acoustic pulse only is taken from Figure 3.5. Other energy in the pulse waveform is not considered. An estimated directivity index of 0.1 dB is also ignored.

The potential energy of the first maximum cavity and the second maximum cavity are computed from the equivalent radii for each as plotted in Figure 3.7 and the assumption of zero pressure within the cavity volumes at their maxima. Both the measurements and the assumption are approximate.

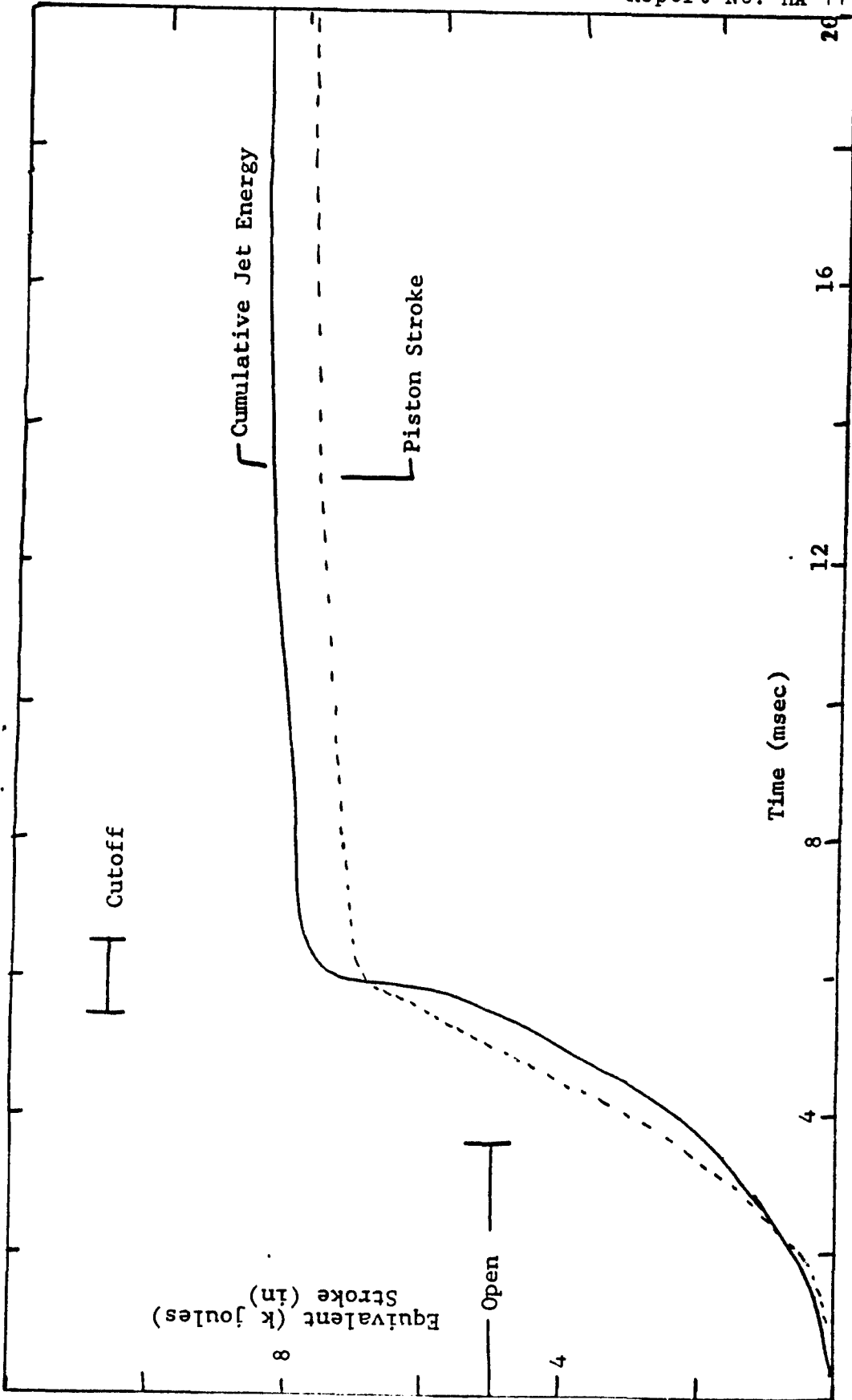


Figure 4.1 Computer Simulation of Jet Energy Accumulation

The acoustical efficiency may be defined as the percentage of the potential energy stored in the maximum cavity which is radiated as acoustical energy in the main positive pulse. Taking the values from Table 4.1, the acoustical efficiency is 44 percent. The overall efficiency from the hydraulic input to the acoustic output of the water gun for the conditions indicated is 4.9 percent.

The least efficient step indicated is 27 percent efficiency in the transformation of the kinetic energy of the jet into the potential energy of the void cavity. It is possible that loss factors within the gun are underestimated in the computer simulation. Nevertheless, improvement in this least efficient step offers a great potential for increasing the overall efficiency of this class of source.

## 5.0 SENECA LAKE MEASUREMENTS

The Hydroshock<sup>(R)</sup> water gun with rectangular ports was selected for the investigation of the effect of greater depth upon the acoustic output of the gun.

Figure 5.1 is one of a number of shallow-depth pressure signatures of the Hydroshock<sup>(R)</sup> water gun with rectangular ports initially recorded at Seneca Lake. The conditions match those of Figure 3.5 except that the measurement hydrophone was located 80 feet beneath the source. The principal events are annotated. Zero time is the point at which the solenoid on the firing valve on the gun is energized. There is pressure evidence that the sleeve valve is starting to open 17 msec later. The positive pressure spike is 30 msec later, immediately followed by the surface reflection.

For the deeper measurements, a double length umbilical was provided which allowed the gun to be lowered to 305 feet maximum. The only adjustment to gun operation was a small increase in the pressure of the air precharge so as to maintain a peak pressure in the air spring when fully cocked which was 2300 psi greater than outside ambient pressure. This insured that the available potential energy stored in the air spring, when cocked and ready to fire, was approximately equal for each depth at which the gun was tested. The calibrated measurement hydrophone was suspended to the depth of the gun at a horizontal separation distance of 156 feet.

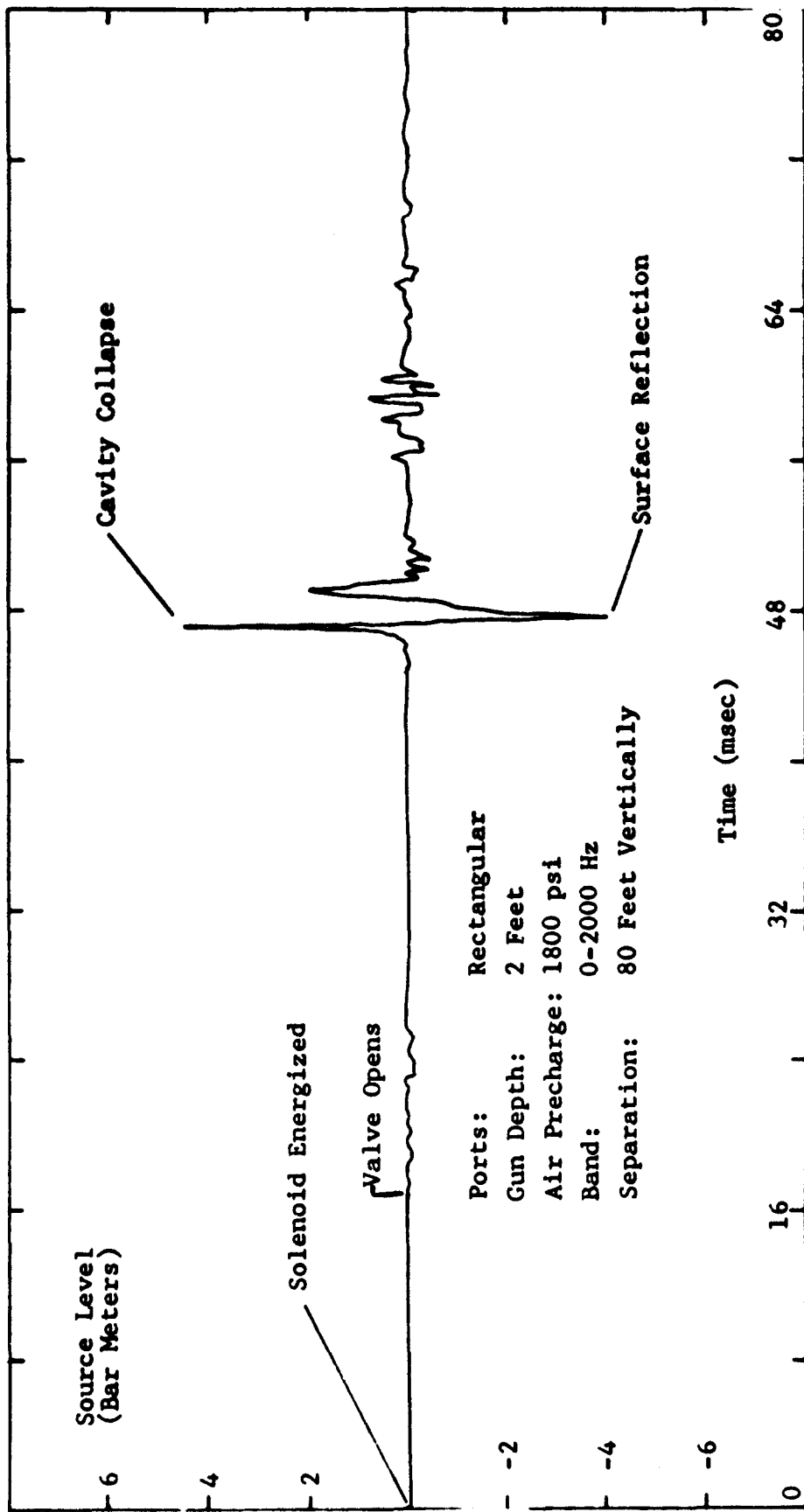


Figure 5.1 Pressure Waveform from the Time of Solenoid Energization

Pressure waveforms recorded with the gun at 90, 150, 210, 280, and 305 feet deep are shown in Figures 5.2 through 5.6 respectively. In Figure 5.2, emission occurs between 25 and 30.5 msec on the time scale. The duration of the negative pressure excursion is about 6 msec. The time from maximum negative pressure to the peak positive pressure is four msec. A small positive pressure spike occurs in the middle of the negative pressure swing at about 36 msec on the time scale. A small positive pressure spike follows the main positive pulse by 3.5 msec. The surface-inverted replicas of the negative-pressure swing and the positive peak each occur delayed 17.5 msec as expected.

As the depth is increased stepwise in succeeding figures to 305 feet in Figure 5.6, several observations may be made. The peak pressure amplitude is inversely proportional to depth. The duration of the positive pressure spike, measured at its half amplitude, dropped from 0.55 msec at 90 feet deep to 0.4 msec at 305 feet deep. The duration of the initial, low-amplitude pressure disturbance associated with the emission has remained constant at about 5.5 msec. The duration of the negative-pressure swing associated with the growth and collapse of the cavity, has dropped from 6.5 msec at 90 feet deep to 2.6 msec at 305 feet deep. The overall time from initial emission to the collapse of the bubble was reduced from 13.2 msec at 90 feet deep to 8.5 msec at 305 feet deep.

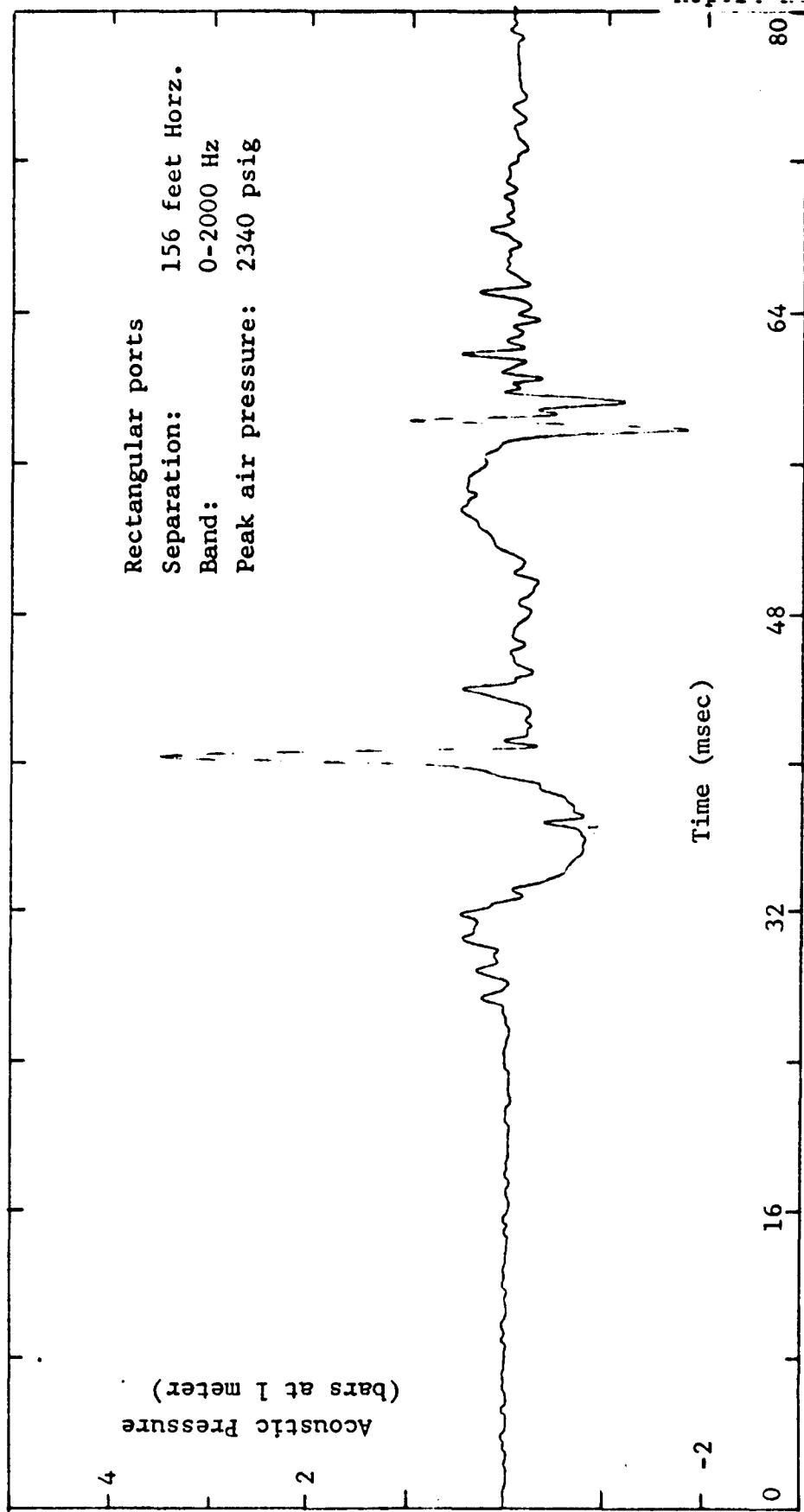
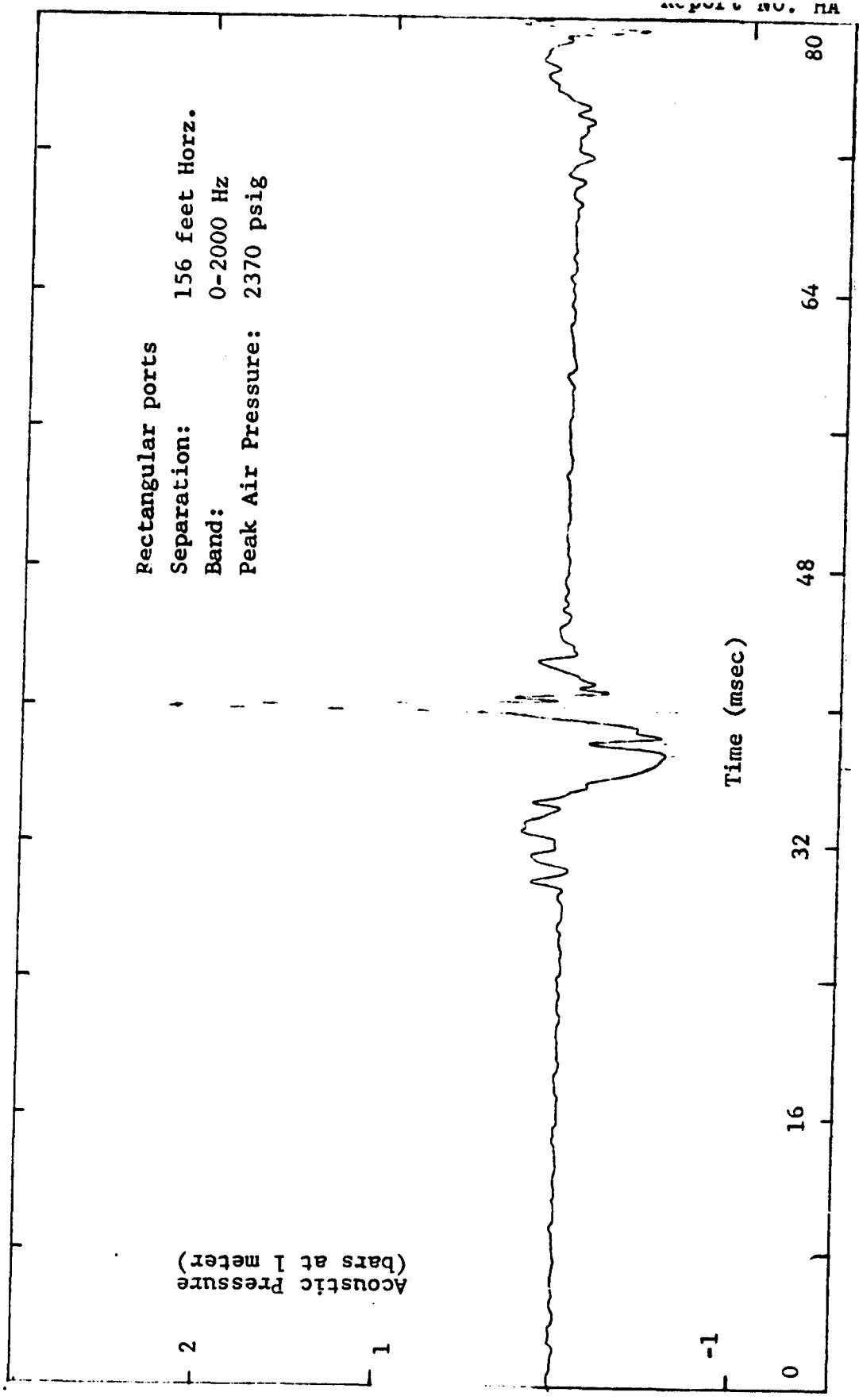


Figure 5.2 Pressure Waveform with Gun 90 Feet Deep



5-5

Figure 5.3 Pressure Waveform with Gun 150 Feet Deep

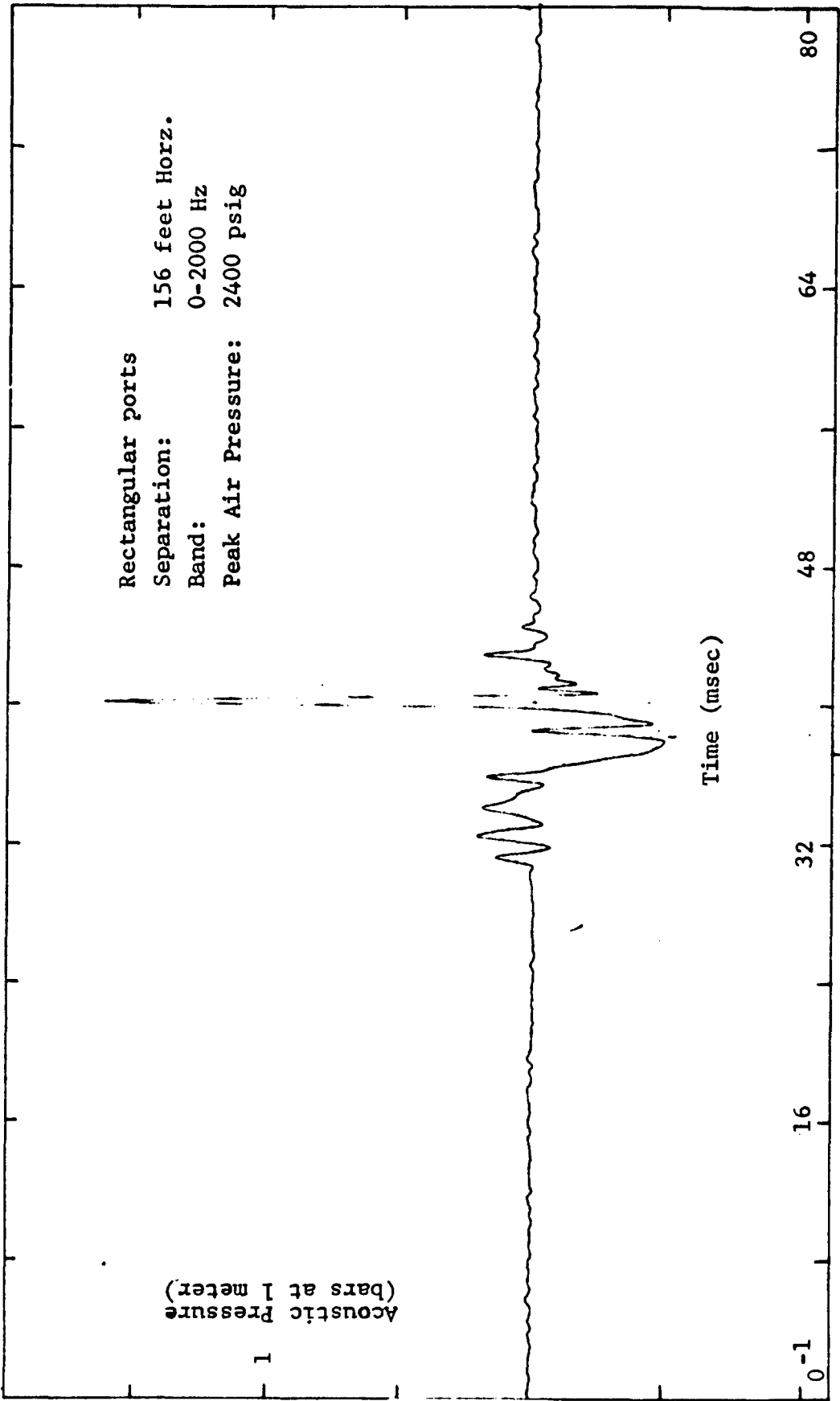
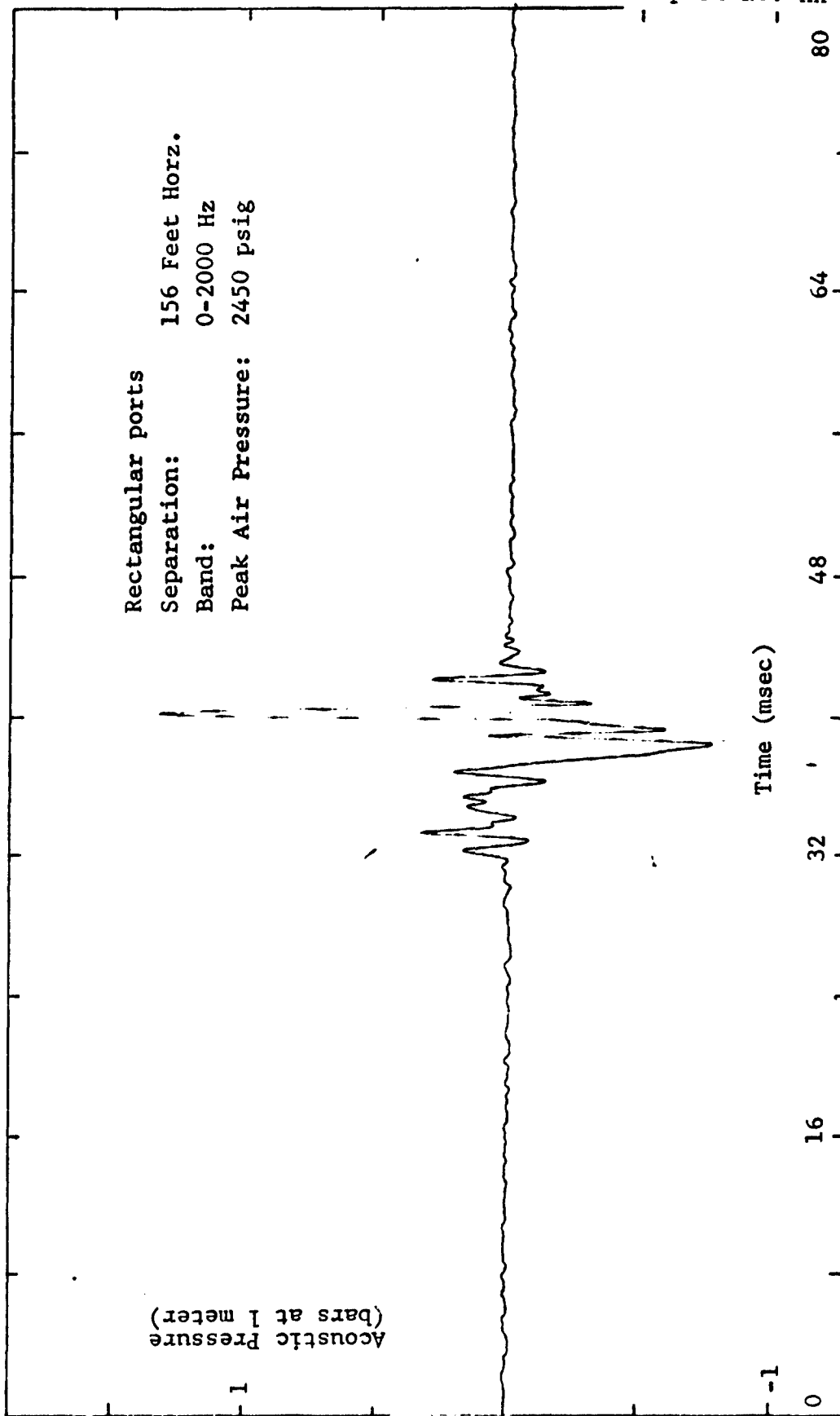


Figure 5.4 Pressure Waveform with Gun 210 Feet Deep



5-7

Figure 5.5 Pressure Waveform with Gun 280 Feet Deep

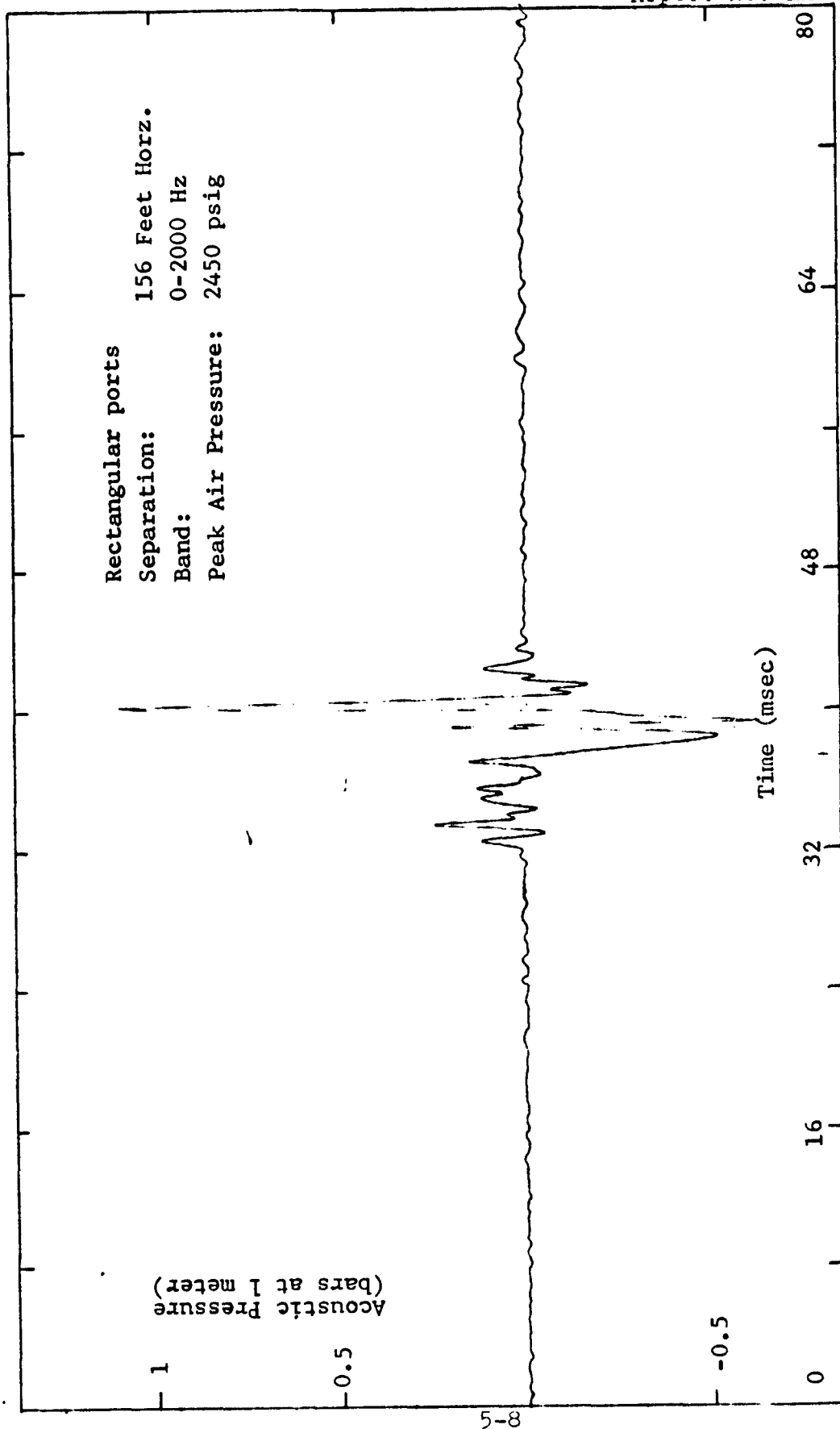


Figure 5.6 Pressure Waveform with Gun 305 Feet Deep

The amplitude of the main positive pressure pulse and the negative pressure swing are reduced by depth. Since the amplitude of the positive pulse within the negative swing remains almost unchanged with depth, its amplitude relative to the other features of the waveform is much enhanced by the 305-foot depth. This stable pulse is believed to be caused by the impact of the sleeve valve on its seat as the sleeve valve recloses the port. (Refer to Figure 2.2.) The tiny secondary pressure pulse trails the main pulse by 2 msec at 305 feet deep instead of the 3.5 msec trail at 90 feet deep. Finally, the surface reflection is no longer in the time window.

While operating at the 210-foot depth, the gun intermittently failed to cock although it fired satisfactorily. The gun was returned to the surface, inspected and a sticky valve corrected.

A plot of peak source level vs. depth is shown in Figure 5.7. Over the depth range from 90 to 305 feet, the peak pressure is reduced 10 dB. From the individual waveforms, we see that much of the acoustic energy is in the main positive pulse. Further, the duration of the positive pulse decreases only slightly with depth. Therefore the square of acoustic energy vs. depth should follow closely the curve of peak acoustic pressure vs. depth.

Included in Figure 5.7 are the peak source levels recorded at shallow depths of 2 to 30 feet with the hydrophone vertically below the gun. Figure 5.1 is one of these records. The peak pressure is less sensitive to depth at these shallower depths.

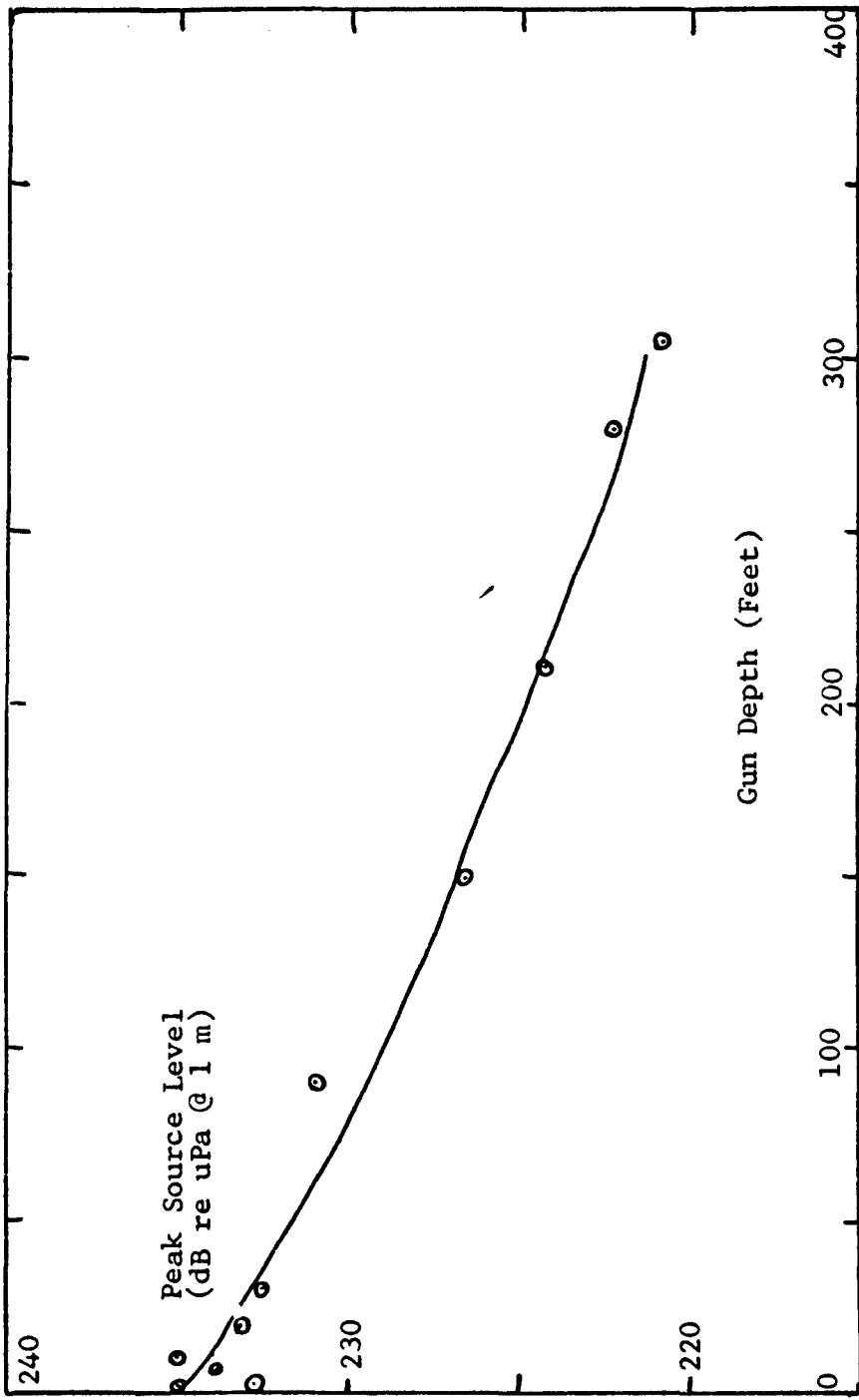


Figure 5.7 Peak Source Level vs. Depth

The dependence of peak source level upon input energy is shown in Figure 5.8. The input energy is approximately proportional to square of the maximum pressure in the air spring which is observed when the gun is cocked. For the indicated conditions at a depth of ninety feet, the peak source level increased about 7.5 dB per air-spring pressure doubled. This effect of air-spring pressure is similar to that observed at shallower depth (Reference 4). It indicates more than a doubling of efficiency for a doubling air-spring pressure.

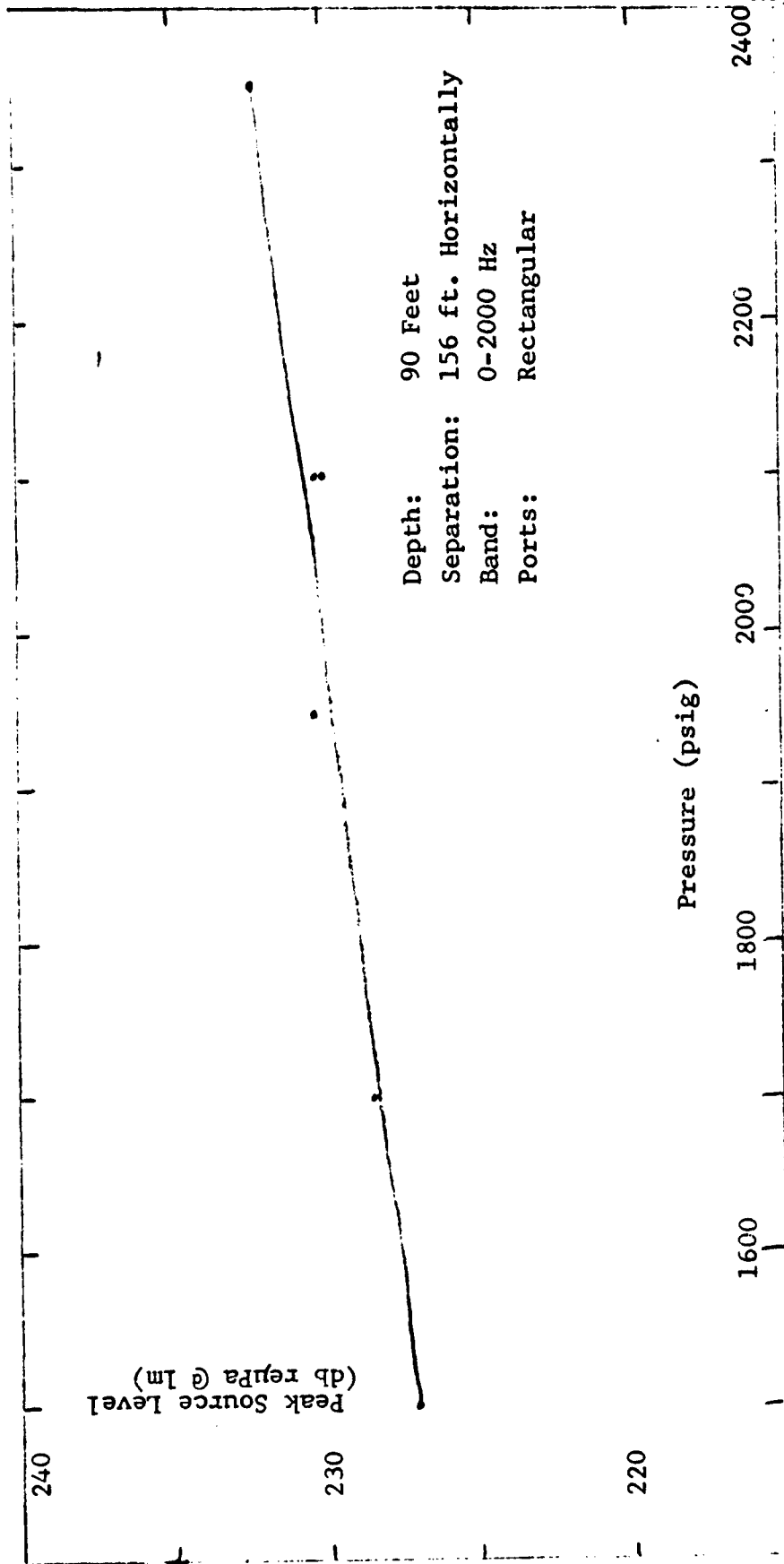


Figure 5.8 Peak Source Level vs. Peak Air-Spring Pressure

## 6.0 DISCUSSION OF RESULTS

One result of this work was the observation in the high-speed movies that the cavitation volume is in the process of formation from the very beginning of the emission of the jet. This cavitation is caused by the turbulence of the jet particularly at its periphery. Vortices which are generated by the shear forces of the high-velocity jet passing through the quiescent water, create local rarified cavities. Coalescence of these local cavities forms the body of cavitation which is observed to grow and then collapse violently. It is believed that the efficiency of the creation of the local rarified cavities requires a relatively high ratio of periphery-to-cross-sectional area in the jet ports.

It was observed in the movie of Figure 3.2 and others, that a regional fragmented portion of a cavitation body appeared to have a life of its own. The fragment grew and collapsed in a manner which seemed independent of its principal neighbor. We conclude that for predictable and uniform performance, it is best if all local cavities associated with one jet do coalesce into and act as a single cavitation body.

Between the two types of ports used in these measurements, the rectangular ports were larger in area (see Table 2.1) and produced a cavitation bubble more spheroidal, less elongated and less fragmented than did the smaller round ports. The larger ports also caused the cavities to be formed closer to the gun. Therefore, the ratio of the porting area to the piston area should be at least as large as was used for the rectangular ports (0.68). The void cavities should not be allowed to form so close to the gun, however, that the gun suffers undue cavitation damage.

Rayleigh's original estimate of the time,  $T_c$ , for total collapse of a spherical bubble in an incompressible fluid (Reference 2) is given by

$$T_c = 0.915 a_0 (\rho_0/P)^{1/2}$$

where

$a_0$  = maximum bubble radius

$\rho_0$  = density

$P$  = static pressure differential for bubble collapse.

Assuming a vacuum within the bubble, the collapse time thus computed for the spheroidal bubble of Figure 3.7 is 9.5 msec. The measured collapse time is 12.2 msec. If the volume of the four bubbles generated by the gun is considered to be a single sphere, the computed collapse time of that sphere is 15.1 msec. The estimates can be improved by consideration of the permanent gas pressure within the bubble.

In the case of the water gun, several factors tend to lengthen the collapse time. Internal water vapor, which would reduce the differential pressure across a given bubble, would increase the collapse time.

The mutual interaction of the other three nearby bubbles from the gun would have a distinct effect in lengthening the collapse time. For shallow gun depths, the interaction of the surface would also extend the collapse time.

A shorter emission time would result in a more uniform age of the individual cavities comprising the large cavitation body. This synchronization should give rise to the growth of a larger maximum cavity volume, a more complete collapse of the cavity and more efficient transformation of bubble energy to acoustic energy. This is another reason for a large ratio of port area to piston area.

A shorter emission time may be especially significant as gun depth is increased since the bubble growth and collapse times are reduced at depth. It presently takes more than 3 msec for the sleeve valve to fully open the ports. A more rapid opening should result in shorter emission time.

Since collapse time may be expressed as

$$T_c = 0.915 a_o (\rho/P)^{1/2}$$

and for a given potential energy, E, in the maximum cavity, the radius of the maximum cavity is

$$a_o = (3 E/4 \rho P)^{1/3}$$

then

$$T_c = (P)^{-5/6}$$

In Figures 5.2 through 5.6, the collapse time was difficult to determine because of the presence of the positive spike in the middle of the negative swing. The relationship of  $T_c$  to P was not constant.

According to Reference 2, both the growth time and the collapse time are proportional to  $(P)^{-5/6}$ . It seems reasonable therefore that the duration of the entire negative swing would be similarly proportional. The predicted ratio of durations for the negative swing between 90 and 305 feet deep is 2.31. The negative duration observed in the figures at 90-foot depth is 6.4 msec and at 305 feet is 2.6 msec. This ratio is 2.46, in good agreement with the predicted ratio.

As shown in Figure 5.7, the peak source level diminished 10 dB as the depth increased from 90 to 305 feet. Thus, source level varied as the inverse square of ambient pressure. It is believed that as ambient pressure increases, the threshold velocity needed to generate a void cavity increases. Since the average jet velocity is unchanged, the proportion of the jet particles which exceed the higher threshold is reduced. This reduces the energy in the cavitation void from which the acoustic impulse is generated.

It was shown in Figure 5.8 that the peak source level increased 7.5 dB as the air spring pressure doubled. This is an increase in efficiency with input energy which is believed to be caused by the higher jet velocity. This results in a higher proportion of jet particle exceeding a threshold velocity required for cavitation and therefore an increased acoustic output.

## 7.0 RECOMMENDATIONS

7.1 We have observed that the collapse time of the cavitation voids from the water gun can be predicted neither by treating each of the four cavities formed as an individual volume nor by considering their total volume as a single cavity. Their proximity to each other causes a significant effect of each on the other. Similar mutual interaction effects have also been observed between guns when two of these guns are within eight feet of each other (Reference 4). At shallow depth, in addition, the effect of the nearby surface is also real. These mutual interaction effects are tractable on an iterative basis.

Therefore, it is recommended that the mutual impedance of four symmetrically-spaced spherical cavities be modeled on the computer. The effect of the surface should be part of this model. This model could be used to predict the interaction between the four cavities from one gun or the effect of guns in an array.

7.2 The use of the water gun, which has been primarily for high-resolution sub-bottom profiling, is now expanding into deeper objectives. This requires larger gun sizes and arrays of the guns. The clean broadband signature available from the water gun has increased its commercial utilization and interest in other applications.

It is recommended that a number of potential applications of interest to the Navy be investigated. Preliminary designs could be developed on a parametric basis to indicate acoustic output, size, weight, power requirements. This would permit their future expansion to additional sizes and operating conditions. Since some of these applications would involve arrays of guns, the recommended mutual impedance model would be utilized in this work.

7.3 From this work, we see that a potential gain in efficiency in the transformation of the kinetic energy of the water jet from gun into the potential energy of the cavitation bubble. There is reason to believe that high efficiency in this transformation is dependent upon a large area of the jet port<sup>a</sup> relative to the area of the piston with a corresponding short emission duration. The efficiency may depend upon how much of the water in the jet is above some threshold velocity which may in turn be dependent upon external ambient pressure. Efficiency may well depend upon how intimately the emerging jet encounters the adjacent quiescent water.

It is therefore recommended that jet configuration be investigated on a relatively simple empirical basis in an effort to increase the gun efficiency significantly. While high-speed photographic techniques can be enlightening in this type of investigation, the ultimate measure of progress is contained in the acoustic signature.

8.0 REFERENCES

1. Bouyoucos, J. V., J. K. McLaughlin, Jr., and R. L. Selsam, "The HYDROSHOCK<sup>(R)</sup> Water Gun", Paper at 50th Annual International Meeting of the Society of Exploration Geophysicists, November 1980.
2. Ross, Donald, Mechanics of Underwater Noise, Chapter 7, Pergamon Press, NY, 1976.
3. Flynn, H.G. Physics of Cavitation in Liquids, Vol. 1, Part B, Chapter 9 of Physical Acoustics, W.P. Mason (Ed), Academic Press, NY 1964 (pp 57 - 172).
4. Bouyoucos, J. V., J. K. McLaughlin, Jr., and R. L. Selsam, "HYDROSHOCK<sup>(R)</sup> Water Gun Arrays", Paper at 51st Annual International Meeting of the Society of Exploration Geophysicists, 1981.

SECTION 9.0 APPENDIX

Theoretical Analysis of a Cavitation Powered Acoustic Generator

H. G. Flynn

---

## A MATHEMATICAL MODEL FOR THE HYDROSHOCK WATER GUN

by

H. J. Flynn

1. INTRODUCTION: A mathematical model for the Hydroshock water gun has been constructed with the general objective of predicting amplitudes of its radiated pressure waves that are in order-of-magnitude agreement with measured values. Specifically, the aim has been to come within a factor of 10 of a measured value of 4 bars at a distance of 1 meter from the device.

The physical device is considered in the analysis as containing a gas chamber and a water chamber separated by a piston. When the gas expands, the piston moves and ejects water through four orifices to form four jets in the surrounding static water medium. In order to make the model one dimensional, it is assumed that, in so far as motion of the piston is concerned, the four orifices which are each of cross-sectional area  $a'$  are equivalent to a single orifice of cross-sectional area  $a = 4a'$ . The jet is assumed to have the same cross-sectional area as the equivalent exit orifice, except as noted below. The jet is at first laminar but soon becomes turbulent.

It is also assumed that the pressure wave radiated by the device is generated by collapsing transient cavities created through decreases in pressure in one or more of the following:

- a. The water chamber
- b. The exit orifice
- c. The laminar section of the jet
- d. The turbulent section of the jet

2. CAVITATION NUCLEI: In order to carry out any reasonable calculation of the radiated pressure wave, it is necessary to specify a distribution of pre-existing gas-filled nuclei in the device and in the jet. These nuclei serve as sites at which pressure decreases can cause transient cavities to grow.

In one mode of operation, water in the Hydroshock water gun is filtered and then held at a high static pressure for several minutes. Under such conditions all large nuclei will quickly disappear and only small bubbles stabilized in some way against diffusion will survive. As will be shown later, nuclei less than a few microns in radius are probably ineffective in producing pressure waves at a distance of 1 meter.

As a consequence nuclei with radii of 5 microns are taken to form the lower limit to the distribution of nuclei. Conditions may be otherwise in the turbulent jet where larger nuclei from the surrounding static medium may be entrained at the jet boundary. Nuclei with radii of 500 microns were chosen as the upper limit on the distribution in the jet. The assumed distribution therefore is one for nuclei with radii  $R_n$  lying in the range:

$$5 \times 10^{-4} \text{ cm.} \quad R_n \quad 5 \times 10^{-2} \text{ cm.}$$

3. MOTION OF THE PISTON: The motion of the piston controls the particle velocity and pressure everywhere in the device and in the jet. Equations that enable us to calculate the speed and position of the piston as a function of time for any specified set of non-dimensional parameters have been derived as the core element of this model. The derivation is given in detail in a report submitted previously (Flynn, 1982).

The set of equations in non-dimensional form is:

$$v^2 = 2 \lambda^{\gamma} (\beta - \xi)^{\gamma-1} \int_0^{\xi} \frac{d\xi'}{(\lambda + \xi')^{\gamma} (\beta - \xi')^{\gamma}}$$

$$\tau = \int_0^{\xi} \frac{d\xi'}{v(\xi')}$$

where  $v$  is the dimensionless speed of the piston,  $\xi$  is the dimensionless displacement of the piston and  $\tau$  is the dimensionless time. The quantities  $\lambda$ ,  $\beta$  and  $\gamma$  are dimensionless parameters defined in the previous report and in the next section.  $\gamma$  is the ratio of specific heats of the gas in the gas chamber.

These equations were derived on the assumption that the liquid is incompressible, the gas is ideal and there are no frictional losses. The equations have been programmed for numerical solution and a specimen calculation for a set of parameters given in the next section is appended as Appendix I.

4. PARAMETERS FOR PISTON MOTION: In calculations made with the use of these equations, it has been assumed that the following values held:

Initial gas volume,  $V_{g0} = 1097 \text{ cm.}^3$

Length of water chamber (stroke of piston),  $L_n = 20.32 \text{ cm.}$

Radius of water chamber,  $k = 3.81 \text{ cm.}$

Radius of exit orifice,  $r' = 0.95 \text{ cm.}$

Radius of equivalent exit orifice,  $r = 2r' = 1.90$  cm.  
 Cross sectional area of water chamber,  $A = 45.6$  cm.<sup>2</sup>  
 Cross sectional area of one exit orifice,  $a' = 2.85$  cm.<sup>2</sup>  
 Cross sectional area of equivalent orifice,  $a = 4a' = 11.40$  cm.<sup>2</sup>  
 Initial static pressure in gun,  $p_0 = 150$  bars  
 Density of water,  $\rho_w = 1$  gm cm.<sup>-3</sup>  
 Density of gas,  $\rho_{go} = 1.90 \times 10^{-2}$  gm cm.<sup>-3</sup>  
 Length of exit orifice,  $L_e = 1.76$  cm.  
 Mass of gas,  $m_g = \rho_{go} V_{go} = 20.79$  gm.  
 Mass of piston,  $m_p = 1179$  gm.  
 Mass of water in exit orifice,  $m_n = \rho_w L_e a = 926.7$  gm.  
 Ratio of specific heats,  $\gamma = 1.4$

With these values, the nondimensional parameters become:

$$\nu = (A/a) = 16$$

$$\lambda = (V_{go}/L_n A) = 1.184$$

$$\beta = 1 + \frac{m_g/3 + m_p + \nu m_n}{\rho_w L_n A} = 2.627$$

The non-dimensional speed  $v$ , the displacement  $\xi$  and the time  $\tau$  are converted into dimensional variables by use of:

$$v_x = v (p_0/\rho_w)^{\frac{1}{2}} = 1.233 \cdot 10^4 v$$

$$t = \tau L_n (\rho_w/p_0)^{\frac{1}{2}} = 1.688 \cdot 10^{-3} \tau$$

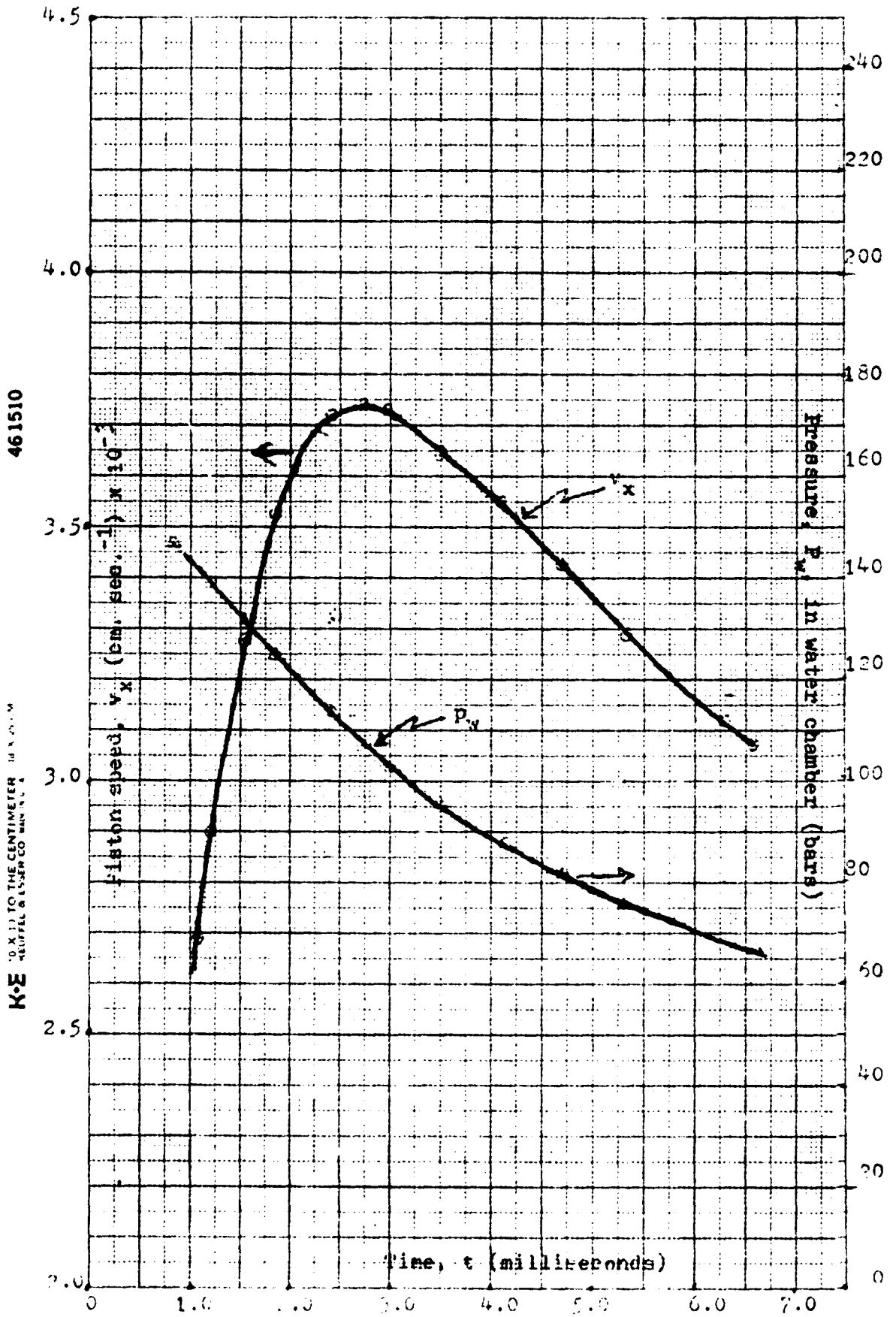
$$x = \xi L_n = 20.32 \xi$$

where  $v_x$  is the speed of the piston in cm. sec.<sup>-1</sup>,  $t$  is the time in seconds and  $x$  is the displacement in cm.

With these parameters, the equations for the piston motion were solved numerically for  $v$  and  $\tau$  as functions of  $\xi$ . Simultaneously, the pressure  $p_w$  in the water chamber (and in the gas chamber) was calculated from:

$$p_w(\xi) = p_{go} \left( 1 + \frac{\xi}{\lambda} \right)^{-\gamma}$$

The corresponding values of  $v_x$  and  $p_w$  computed from Appendix I) are plotted in Fig. 1 as functions of the time  $t$ .



REPRODUCED FROM  
BEST AVAILABLE COPY

Once we know  $v_x$  as a function of time  $t$ , we can find the time dependent pressure both within the device and in the jet. The next step then is to see whether the pressure drop anywhere is enough to generate transient cavities from the available nuclei. Calculations of the maximum pressures within collapsed cavities have been made using a set of computer programs that compute the growth and collapse of cavities from any specified nucleus,  $R_n$ , when it is acted on by a specified time dependent pressure,  $P_A(t)$ .

The solutions generated by these programs are based on the assumption that a cavity that is spherical at its maximum radius will retain its spherical shape throughout collapse. However, collapsing cavities may breakup during collapse and the pressures found in these solutions should be regarded as a relative measure rather than an absolute value.

5. CAVITATION WITHIN THE WATER GUN: The pressure drop within the water chamber and the exit orifice will not generate transient cavities despite the pressure drop of 90 bars shown in Fig. 1. Numerical calculations show that nuclei simply expand and contract in equilibrium with the transient pressure. The reason is that even with a rapid decrease of pressure from its initial value, the time interval which is of the order of several milliseconds, is very long compared with the resonance period of any nuclei in the assumed distribution. Nuclei expand at most to several times  $R_n$  and cavity collapse does not occur.

6. CAVITATION IN THE LAMINAR JET: The pressure in an axially symmetric jet in a medium at rest has a minimum  $p_c$  at the center of the jet (Lai, 1954). The fall in pressure is given by the equation (Lai, Eq. 5.56):

$$p_c - p_L = - 0.00295 (\rho_w v_m^2 / 2)$$

where  $p_L$  is the static pressure in the liquid and the speed of the jet is related to the piston speed  $v_x$  by:

$$v_m = (A/a') v_x = 4 v_x$$

In the computation of the piston motion, the use of an equivalent exit orifice with a cross sectional area equal to those of the four exit orifices is an appropriate approximation. The calculated piston speed  $v_x$ , shown in Fig. 1, has a maximum value of  $3.74 \times 10^3$  cm. sec.<sup>-1</sup>. For this value of  $v_x$ , the jet speed would be  $v_m = 1.5 \times 10^4$  cm. sec.<sup>-1</sup> and the pressure drop would be:

$$P_C - P_L = -0.33 \text{ bars}$$

7. CAVITATION IN THE TURBULENT JET: We now must show that pressure fluctuations in the turbulent jet are large enough to generate transient cavities from nuclei lying in the assumed distribution.

Turbulence is inherently a random phenomenon and statements made about a turbulent region are always statements about the probability of an event. Fortunately there are some relatively simple formulae that let us derive all the information we need from a knowledge of the particle speed  $v_m$  in the jet. The relation of  $v_m$  to the piston speed  $v_x$  is the same as that in the laminar part of the jet; that is,  $v_m = (\Lambda/a) v_x$  and hence in this calculation  $v_m = 4 v_x$ .

The crucial parameter is the quantity,  $\sigma$ , the root-mean-square value of the pressure fluctuation,  $\Delta p$ . This parameter is the most probable fluctuation that will occur. Values of  $\sigma$  may be determined from the following equation (Esipov and Naugol'nykh, 1975):

$$\sigma = \pm \left[ \overline{(\Delta p)^2} \right]^{1/2} = \pm 0.056 (\rho_w v_m^2 / 2)$$

The plus and minus signs are essential because a negative value is as probable as a positive value. Negative values of  $\Delta p$  with magnitudes greater or less than  $\sigma$  may occur with lesser probability. Thus  $\sigma$  gives us the most likely negative pressure fluctuation generated by a jet speed  $v_m$ .

We now must determine the time duration of a pressure fluctuation with a magnitude  $\sigma$ . We assume that the pressure fluctuations have a Gaussian distribution of the form:

$$f(\Delta p) = \frac{1}{\sqrt{2\pi}} \frac{1}{\sigma} e^{-\frac{(\Delta p)^2}{2\sigma^2}}$$

where  $F(\Delta p)$  is the probability that the pressure  $p(t)$  at any instant is in the range  $(p, p + \Delta p)$ . This equation can be used to determine the average value of  $T$ , the time between zero crossings of  $\Delta p$ . This average value  $\bar{T}$  has a reciprocal  $\bar{f}$  that is the average frequency associated with a given value of  $v_m$ . An estimate of  $\bar{f}$  is given by the following range (Franklin and McMillan, 1980):

$$0.01 \leq (\bar{f}d/v_m) \leq 0.04$$

where  $v_m$  is the jet speed,  $d$  is the diameter of the exit orifice ( $d = 2r'$ ). Then at the lower limit (where  $\bar{f}$  is a minimum and  $\bar{T}$  is a maximum), the average period of a fluctuation is given by:

$$\bar{T} = 100d/v_m$$

8. GENERATION OF TRANSIENT CAVITIES IN THE TURBULENT JET: We are now in a position to calculate the most probable negative pressure fluctuation and its probable duration for the specific example at hand. We find that for  $v_x = 3.74 \times 10^3$  cm. sec.<sup>-1</sup> and hence  $v_m = 1.5 \times 10^4$  cm. sec.<sup>-1</sup>,

$$\sigma = -100.3 \text{ bars and } \bar{T} = 3.3 \times 10^{-3} \text{ sec.}$$

These values of  $\sigma$  and  $\bar{T}$  suggest that we may represent a pressure fluctuation in the turbulent jet by a Gaussian pulse of amplitude  $P_A = -6.26$  bars and a FW =  $10^{-4}$  sec. Calculations have been made of the growth and collapse of transient cavities generated by such pressure pulses on nuclei at the lower and upper limits of the nuclei distribution. Pressure amplitudes of -5 and -10 bars were also used. Once the maximum collapse pressure at a minimum radius  $R_m$  is found, the radiated pressure amplitude  $p_f$  at 1 meter can be found from the relation:

$$p_f = p_m R_m$$

when  $R_m$  is given in meters.

The calculated values of the maximum radius,  $R_o$ ; the minimum radius  $R_m$ , the maximum collapse pressure  $p_m$  and the radiated pressure amplitude  $p_f$  at 1 meter are presented in the following tables:

$R_n = 5 \text{ microns}$

$P_A$ (bars)	$R_o/R_n$	$R_m/R_n$	$p_m$ (bars)	$p_f$ (bars)	$R_o/R_m$
-5	98.3	0.135	$8.07 \times 10^4$	0.054	731
-10	561.2	0.144	$5.28 \times 10^5$	0.381	3892
-100	7514	0.150	$1.50 \times 10^6$	1.12	$4 \times 10^4$

$R_n = 500 \text{ microns}$

$P_A$ (bars)	$R_o/R_n$	$R_m/R_n$	$p_m$ (bars)	$p_f$ (bars)	$R_o/R_m$
-5	6.1	0.380	$1.45 \times 10^3$	0.275	16
-10	10.9	0.300	$7.82 \times 10^3$	1.17	36
-100	16.8	0.303	$7.04 \times 10^4$	10.7	253

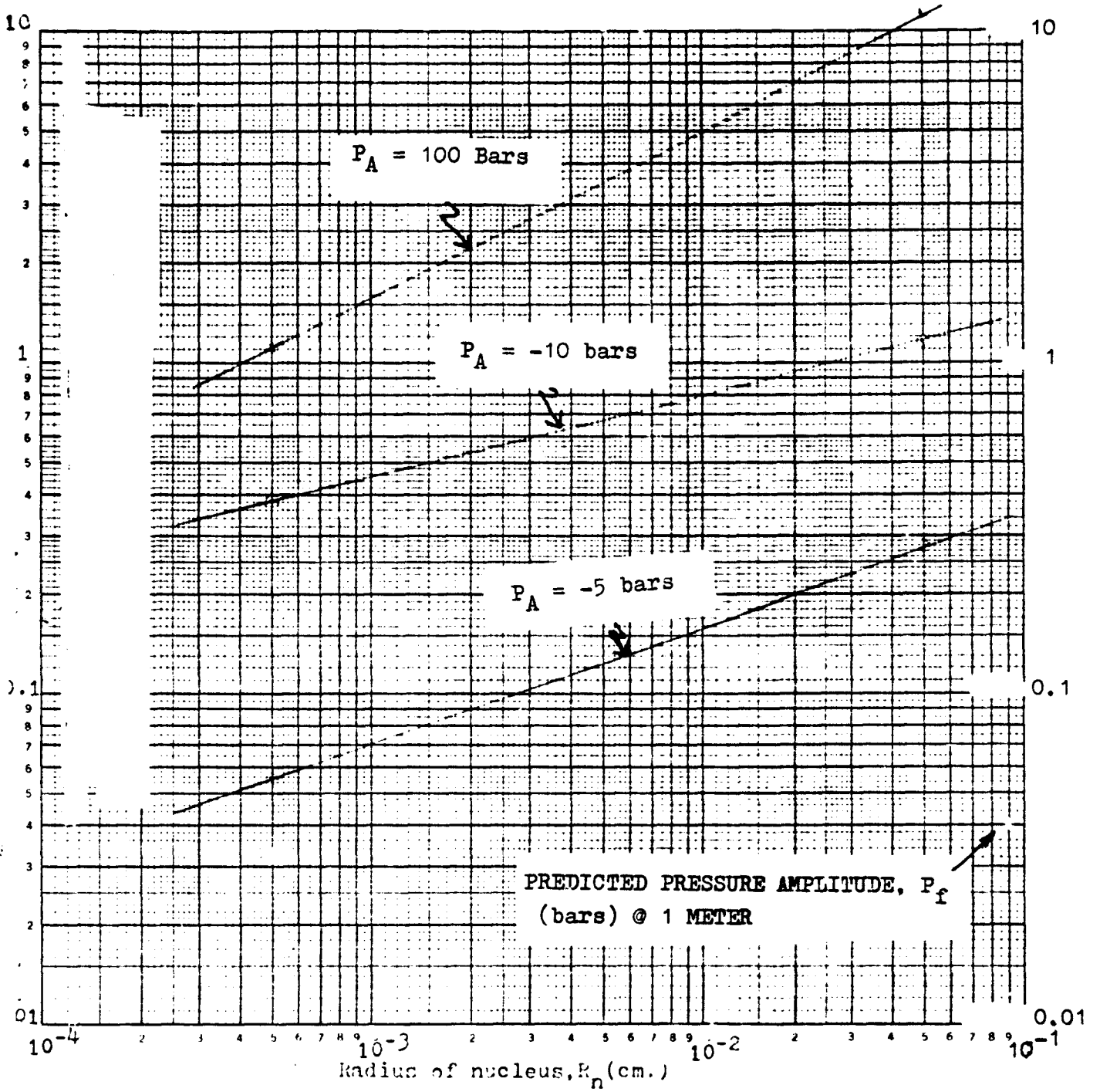
9. DISCUSSION: These tables show that the most probable pressure fluctuations in the turbulent region of the jet generate values of radiated pressure  $p_f$  close to the measured pressures. Further transient cavities that grow from nuclei at the upper limit of 500 microns have both larger values of  $p_f$  and smaller ratios  $R_o/R_m$ . Hence predictions about transient cavities starting from the 500 micron nuclei are more reliable than those starting from 5 micron nuclei. These relationships are evident in Fig. 2.

It is apparent from the structure of the equations governing the piston motion that the parameter

$$\mathcal{V} = (A/a)^2$$

is probably the most important one of the non-dimensional set because it appears as an exponent.

Fig. 2



The parameter  $\lambda = V_{g0} / aL_n$  is the ratio of the initial volume of the gas to the initial volume of water in the water chamber, while the parameter B is essentially the ratio of the mass of gas, the mass of the piston and the mass of water in the exit orifice to the initial mass of water in the water chamber. The computer program developed for solution of the equations of piston motion make<sup>s</sup> it relatively easy to study the effect of varying these parameters on the piston speed  $v_x$  and hence on cavitation generated in the turbulent jet.

The analysis that resulted in these equations assumed that the orifices closed and opened instantaneously. Obviously when the orifices open and close in a finite time interval, the area  $a$  changes with time and the parameter  $\nu$  becomes also time dependent.

As the orifice decreases in area,  $\nu$  becomes very large and frictional losses could be a limiting factor. Such losses could be introduced in the equations for piston motion if we assume that losses in the orifice are proportional to  $e'v_m^3$  where  $e'$  is an experimental constant. Then a new dimensionless parameter  $e$  would appear, where:

$$e = 2e' / \rho_w A$$

and is additive to  $\nu$  in the form

$$(\nu - e)$$

This frictional force will modify the amplifying effect of the area ratio ( $A/a$ ) as one would expect. The effect of finite closing times could be handled in obtaining numerical solutions by considering small intervals of  $x$  or  $t$  in which  $(\nu - e)$  is taken to be constant.

Calculations of the speed in the turbulent jet have been based on the assumption that the diameter of the jet is approximately that of the exit orifice. This assumption most likely overestimates values of  $v_m$  and hence the values of  $\sigma$ . One justification for assuming that the jet is a cylinder of diameter  $d = 2r'$  is that the jet can always be forced to take on such a configuration by proper design of the exit orifice. The value of  $v_m$  would then be the maximum obtainable from a specified pair of  $v_x$  and  $r'$ . Photographs taken by Hoyt and Taylor clearly show this cylindrical structure (Hoyt and Taylor, 1952)

REFERENCES

1. H. G. Flynn, Report to Hydroacoustics, Inc., dated 20 Dec. 1983
2. I. B. Esipov and K. A. Naugol'nykh, "Cavitation noise in submerged jets," Sov. Phys. Acoust. 21 404(1975)
3. Shih-I Pai, Fluid Dynamics of Jets, D. Van Nostrand Co., Inc., New York, 1954, p. 108.
4. R. E. Franklin and J. McMillan, "Noise generation in cavitating flows: Part 2, The submerged jet." Report OUEL-1313/80 Pt.2, Engineering Laboratory, Oxford University, UK, 1980.
5. J. W. Hoyt and J. J. Taylor, "Water-jet photography," Naval Research Reviews, 34 3 (1982)

REPORT DOCUMENTATION PAGE		READ INSTRUCTIONS BEFORE COMPLETING FORM
1. REPORT NUMBER HA 111-83	2. GOVT ACCESSION NO. <b>A134597</b>	3. RECIPIENT'S CATALOG NUMBER
4. TITLE (and Subtitle) Final Report On Hydroshock <sup>(R)</sup> Water Gun Research	5. TYPE OF REPORT & PERIOD COVERED Final	
7. AUTHOR(s) J. K. McLaughlin, Jr.	6. PERFORMING ORG. REPORT NUMBER HA 111-83	
9. PERFORMING ORGANIZATION NAME AND ADDRESS Hydroacoustics Inc. P.O. Box 23447 Rochester, NY 14692	8. CONTRACT OR GRANT NUMBER(s) N00014-82-C-0647	
11. CONTROLLING OFFICE NAME AND ADDRESS Office of Naval Research 800 N. Quincy St. Arlington, Virginia 22217	10. PROGRAM ELEMENT, PROJECT, TASK AREA & WORK UNIT NUMBERS	
	12. REPORT DATE April 5, 1983	
14. MONITORING AGENCY NAME & ADDRESS (if different from Controlling Office)	13. NUMBER OF PAGES 59	
	15. SECURITY CLASS. (of this report) Unclassified	
16. DISTRIBUTION STATEMENT (of this Report)		
Unlimited/Unclassified		<b>DISTRIBUTION STATEMENT A</b> Approved for public release Distribution Unlimited
17. DISTRIBUTION STATEMENT (of the abstract entered in Block 20, if different from Report)		
18. SUPPLEMENTARY NOTES		
19. KEY WORDS (Continue on reverse side if necessary and identify by block number) Acoustic source, water gun, cavitation bubble, depth, high-speed underwater movies.		
20. ABSTRACT (Continue on reverse side if necessary and identify by block number) The report describes an investigation of the mechanisms which control the performance of the water gun as an acoustic source. Employed in this study was the Hydroshock <sup>(R)</sup> water gun which utilizes water under high pressure as its prime power. This class of underwater source delivers a clear broadband acoustic signal which is desirable in target strength measurement and in acoustic profiling. Upon actuation, the gun emits		

four simultaneous high velocity jets of water. Each jet forms a cavitation bubble which subsequently collapses violently generating a high amplitude acoustic transient.

High speed movies were used to study the formation and collapse of the cavitation bubble generated by one of the four water jets. The formation of the cavitation bubble occurred during the entire period of the water jet emission. The collapse time of each of the four individual cavitation bubbles generated by the gun was lengthened by the mutual interaction of the three neighboring cavities. Over the depth range of 90 to 305 feet, the growth and collapse time were observed to be proportional to  $P^{-5/6}$ , where P is the absolute static head at the gun.

A predictive model of the far-field acoustic pressure radiated by the water gun, based upon preexisting gas-filled nuclei in the jet fluid, is presented in the Appendix.